

AD/A-004 324

INVESTIGATION OF LIFT, DRAG, AND AERO-
DYNAMIC PITCHING MOMENT DURING IN-
FLIGHT RECOVERY OF A REMOTELY PILOTED
VEHICLE

Jon L. Gross

Air Force Institute of Technology
Wright-Patterson Air Force Base, Ohio

September 1973

DISTRIBUTED BY:

NTIS

National Technical Information Service
U. S. DEPARTMENT OF COMMERCE

UNCLASSIFIED

Security Classification

AD/A-004324

DOCUMENT CONTROL DATA - R & D

(Security classification of title, body of abstract and indexing annotation must be entered when the overall report is classified)

1. ORIGINATING ACTIVITY (Corporate author)		2a. REPORT SECURITY CLASSIFICATION	
Air Force Institute of Technology (AU) Wright-Patterson Air Force Base, Ohio 45433		UNCLASSIFIED	
		2b. GROUP	
3. REPORT TITLE			
"INVESTIGATION OF LIFT, DRAG, AND AERODYNAMIC PITCHING MOMENT DURING IN-FLIGHT RECOVERY OF A REMOTELY PILOTED VEHICLE"			
4. DESCRIPTIVE NOTES (Type of report and inclusive dates)			
AFIT Thesis			
5. AUTHOR(S) (First name, middle initial, last name)			
Jon L. Gross Capt USAF			
6. REPORT DATE		7a. TOTAL NO. OF PAGES	7b. NO. OF REFS
September 1973		99	11
8a. CONTRACT OR GRANT NO.		9a. ORIGINATOR'S REPORT NUMBER(S)	
b. PROJECT NO.		GAW/AE/74-2	
c.		9b. OTHER REPORT NO(S) (Any other numbers that may be assigned this report)	
d.			
10. DISTRIBUTION STATEMENT			
Approved for public release; distribution unlimited.			
11. SUPPLEMENTARY NOTES		12. SPONSORING MILITARY ACTIVITY	
Approved for public release; IAW AFR 190-17 JERRY C. HIX, Captain, USAF Director of Information		Air Force Institute of Technology Wright-Patterson AFB, Ohio 45433	
13. ABSTRACT			
<p>A potential approach for recovery of remotely piloted vehicles (RPV) is the in-flight docking of the RPV with a mothership. Some design concepts are presented for in-flight recovery systems. A steady aerodynamic analysis was performed on a hypothetical RPV as it approached the mothership for docking. The correct trend in the variation of lift and static pitch moment of the RPV was predicted using a horseshoe vortex model to represent the mothership.</p>			

Reproduced by
NATIONAL TECHNICAL
INFORMATION SERVICE
U S Department of Commerce
Springfield VA 22151

PRICES SUBJECT TO CHANGE

DD FORM 1 NOV 65 1473

UNCLASSIFIED
Security Classification

INVESTIGATION OF LIFT, DRAG, AND
AERODYNAMIC PITCHING MOMENT DURING IN-
FLIGHT RECOVERY OF A REMOTELY PILOTED VEHICLE

THESIS

Presented to the Faculty of the School of Engineering
of the Air Force Institute of Technology
Air University
in Partial Fulfillment of the
Requirements for the Degree of
Master of Science
by

Jon L. Gross, B.S.A.E.

Captain USAF

Graduate Aerospace Engineering
September 1973

Approved for public release; distribution unlimited.

14

Preface

In this thesis, I have proposed a system for in-flight fixed wing recovery of remotely piloted vehicles (RPV). The concept of in-flight recovery of one aircraft by another is not original. This concept dates back to the 1930's when the Curtis F9C-2 Sparrowhawk was operated from a trapeze attached to the U.S.S. Akron dirigible. In the late 1940's and early 1950's, two parasite fighter projects resulted in a few dockings with another aircraft. In developing the proposed in-flight recovery system for RPV's, I have drawn upon these parasite fighter programs.

To analyze the aerodynamic interference between the capturing aircraft and the RPV, I developed a horseshoe vortex model to represent the capturing aircraft. The development of this model follows the development presented by Glauert. With the aid of the horseshoe vortex model, I calculated the static change in lift, drag, and pitching moment on the RPV at various points along a flight path to the docking point.

I thank Professor Harold C. Larsen, Director, Air Force Institute of Technology Aerospace Design Center, for his guidance and assistance during the preparation of this thesis. This thesis is dedicated to my wife for her understanding and support during its preparation.

Contents

	<u>Page</u>
Preface	ii
List of Figures	iv
List of Symbols	v
Abstract.	vi
I. Introduction	1
II. Design Concepts.	4
Fixed Wing RPV	4
Oblique Wing RPV	5
Capture System	6
Skyhook.	10
Trapeze.	13
Aft Support, Fixed Wing RPV.	13
Aft Support, Oblique Wing RPV.	16
III. Horseshoe Vortex Model of Mothership	17
Contribution of Bound Vortex	20
Contribution from Trailing Vortices.	21
Calculation of \vec{q}_2	22
Calculation of \vec{q}_3	23
Total Induced Velocity	24
Analysis of Induced Velocity	25
IV. Steady State Analysis of Aerodynamic Interference.	30
Variation of Lift.	32
Variation of Drag.	35
Variation of Pitch Stiffness	36
Analysis of Hypothetical RPV	41
V. Conclusions and Recommendations.	56
Conclusions.	56
Recommendations.	56
Cited References.	57
Appendix A: Computer Program	58
Vita.	90

List of Figures

<u>Figure</u>	<u>Page</u>
1 Oblique-Winged RPV	5
2 RPV Capture System (Bomb Bay Doors).	7
3 RPV Capture System (Aft Doors)	8
4 Fixed-Wing RPV with Skyhook Extended	10
5 Skyhook.	11
6 Bomb Bay Trapeze	13
7 Aft Door Trapeze	14
8 Mothership Horseshoe Vortex.	17
9 Induced Velocity Distribution, $U_{\infty} = 300$ Knots.	25
10 Induced Velocity Distribution, $U_{\infty} = 200$ Knots.	26
11 RPV Flight Path.	30
12 Steady Level Flight of RPV	32
13 Definition of Angles	33
14 Definition of Pitch Moment Parameters.	38
15 Velocity Change of RPV	44
16 Lift Change of RPV	45
17 Change in RPV Coefficient of Lift.	46
18 Angle of Attack Change	47
19 Change in Coefficient of Drag.	48
20 Drag Change of RPV	49
21 Thrust Change of RPV	50
22 Change in RPV Static Pitch Stability	52
23 Closing Velocity	53
24 Time to Dock	54
25 Simplified Flow Diagram.	59

List of Symbols

$a = C_{L\alpha}$	Lift Curve Slope
AR	Aspect Ratio
\bar{c}	Mean Aerodynamic Chord
c.g.	Center of Gravity
C_D	Coefficient of Drag
C_{D0}	Coefficient of Drag at Zero Lift
C_L	Coefficient of Lift
C_M	Moment Coefficient
$C_{M\alpha}$	Derivative of Static Pitch Moment with Respect to α
D	Drag
e	Oswald Airplane Efficiency Factor
h	Location of c.g. (Fig. 14, p. 38)
h_{nw}	Location of wing mean aerodynamic center (Fig. 14, p. 38)
i_t	Tail Incidence Angle
k	Correction Factor in Coefficient of Drag
l_t	Distance Between c.g. and Tail Aerodynamic Center
\bar{l}_t	Distance Between Wing Aerodynamic Center and Tail Aerodynamic Center
L	Lift
M	Moment
$P(X1, Y1, Z1)$	Point of Analysis (Location of RPV)
\vec{q}_1	Induced Velocity from Bound Vortex
\vec{q}_2	Induced Velocity from +s' trailing Vortex
\vec{q}_3	Induced Velocity from -s' Trailing Vortex
$\vec{r}_1, \vec{r}_2, \vec{r}_3$	Vectors Defined in Fig. 8, p. 17
R	Ratio s'/s

s	Semi-span of Wing
s'	Semi-span of Trailing Vortex Filaments
S	Wing Area
z	Wing Offset from c.g. (Fig. 14, p. 38)
z_t	Tail offset from c.g. (Fig. 14, p. 38)

Subscripts

ac	Aerodynamic Center
t	Tail
W	Wing
∞	Free Stream Condition

Greek Letters

α	Angle of Attack
α_{Lo}	Angle of Attack Zero Lift
α_{∞}	Free Stream Angle of Attack
ϵ	Downwash Angle from RPV Wing
Γ_o	Circulation Around Mid-span of Wing
$\Gamma(y)$	Elliptic Variation of Circulation on Wing Span
ρ	Density at Altitude
ρ_o	Density at Sea Level
τ	Angle Between Relative Velocity and Free Stream Velocity (Fig. 13, p. 33)

Abstract

A potential approach for recovery of remotely piloted vehicles (RPV) is the in-flight docking of the RPV with a mothership. Some design concepts are presented for in-flight recovery systems. A steady aerodynamic analysis was performed on a hypothetical RPV as it approached the mothership for docking. The correct trend in the variation of lift and static pitch moment of the RPV was predicted using a horseshoe vortex model to represent the mothership.

I. Introduction

Recent articles in the open literature indicate numerous advantages of using Remotely Piloted Vehicles (RPV's) in place of piloted vehicles. One of the main advantages of using RPV's is that they can operate in a desired area without potential loss of a pilot. One of the major disadvantages in using RPV's is the number of personnel and amount of equipment presently required to launch and recover a single RPV. During the present Department of Defense budget limitations, total funds available are remaining relatively constant while the manpower costs are rising rapidly. By reducing the number of personnel required to recover RPV's, the cost of RPV operations may be decreased.

For the RPV's that are air launched from a "mother" aircraft, it may be more cost effective to have the launch aircraft also act as the recovery system. Under current practices the launch and recovery systems are completely separate and distinct. The development of a integrated launch/recovery system provides the potential for a cost savings by reducing the number and type of land, air, or water vehicles required to carry out RPV operations.

One possible concept for an integrated launch/recovery system is in-flight capture of the RPV by a fixed wing aircraft. Mid-air capture of one aircraft by another aircraft is not a new concept. Both the XF-85 and the XF-84 projects of the late 1940's and early 1950's showed that it was physically possible for one aircraft to rendezvous and dock with another aircraft. However, both programs showed that mid-air rendezvous and docking was not simple. As the docking aircraft approached the capture mechanism of the mother aircraft, the aerodynamic interference between the two aircraft drastically increased the occurrence of adverse

effects on the docking aircraft which was much smaller than the mother aircraft. The drag on the docking aircraft increased making it difficult to maintain a steady closing speed. A degradation in the stability of the docking aircraft occurred as the capture mechanism was approached.

Before flight tests are performed on potential launch/recovery systems, an analysis of the aerodynamic interference between the aircraft involved should be performed. Capture wind tunnel tests should be performed to verify the analysis or provide data for the analysis. The redesign necessary as a result of flight testing may be minimized by performing an analysis and wind tunnel test of the aerodynamic interference before the aircraft is built or modified.

The objective of this thesis is to perform a steady state aerodynamic analysis of the interference between the two aircraft of a proposed integrated launch/recovery system for RPV's. In this thesis, some design concepts for the equipment necessary for in-flight docking of a fixed wing and oblique wing RPV are proposed. In the analysis of the aerodynamic interference the mothership wing is modeled by a horseshoe vortex system with elliptical distribution of lift on the wing. The fuselage and tail effects on the mothership on the RPV are neglected in the analysis.

The analysis of the interference between the two aircraft consists of computing the steady state values of RPV lift, drag, and aerodynamic pitch moment at positions relative to the mothership as the point of analysis is moved to the docking point. The thesis is divided into three major areas:

- a. Design concepts
- b. Horseshoe vortex model of mothership
- c. Steady state analysis of aerodynamic interference

II. Design Concepts

Aerial capture of one aircraft by another is not a new concept. The author has found in the literature three systems which were designed for and performed aerial capture. The first system, the Curtiss F9C-2 Sparrowhawk, was operated from a trapeze installation aboard the U.S.S. Akron dirigible in 1933. The second system was the XP-85 "GOBLIN" designed by McDonnell Aircraft Corporation (1944-1949). The XP-85 was designed as a parasite fighter to be carried internal to the B-36. Only two XP-85 prototype were built and flight tested. The third system was the F-84F FICON, also designed to be carried by the B-36. The FICON was a modified Republic F-84 which was flight tested in March 1953. In addition, F-84 aircraft were designed to be wing tip carried on the B-50, but successful "hook-on" of two aircraft was never made.

In the discussion of design concepts for in-flight recovery of RPV's, two different types of aircraft will be discussed. The first type of RPV is a fixed wing aircraft and the second is an oblique wing RPV on which the wing pivots as a unit.

Fixed Wing RPV

The fixed wing RPV recovery is based on aircraft like the Firebee drone. The Firebee drone aircraft has the wing fixed to the fuselage. For fixed wing RPV's, some mechanism will most likely have to be added to the wings to allow them to fold for storage inside the mothership. The F-85 project used a folding mechanism on its wings so that it could be stored in the bomb bay of the B-36.

Oblique Wing RPV

Discussion of oblique wing RPV recovery is based on an aircraft that

has its wing mounted on a pivot. The pivoted wing allows the complete wing to be rotated so that it is parallel to the fuselage, thus decreasing the wing span for storage inside the mothership.

Some of the advantages for using oblique winged aircraft are presented in an article by Robert T. Jones (Ref 1:66-70). Jones proposed a oblique-winged aircraft as a candidate for the Super Sonic Transport. The oblique-wing of his proposed aircraft pivots as a unit to different oblique angles corresponding to flight at different Mach numbers. Jones gives the following advantages for an oblique-winged aircraft:

- a. The maximum lift-drag ratio for various Mach number ranges are "significantly higher than those previously obtained with arrow wing or delta wing body combinations."
- b. The oblique elliptic wing has the optimum supersonic wing planform indicated by the drag reversibility theorem of Von Karman and Hayes.
- c. The wing structure is continuous across the pivot producing only a tension load on the pivot with none of the bending loads of the "swing wing."
- d. Turning the wing as a whole does not cause a rearward shift of the center of lift because the centroid of area does not move relative to the center of gravity.
- e. The optimum fuselage shape for the oblique-wing, which conforms to the "area rule," is nearly cylindrical as compared to the localized deep indentation of the fuselage for the swept wing.

An oblique-winged aircraft of the type discussed by Jones is proposed for use with the integrated launch/recovery system discussed in this thesis (Fig. 1, p. 5). The pivoted oblique-wing will allow the RPV to fly with the wing straight for capture at subsonic speed and to

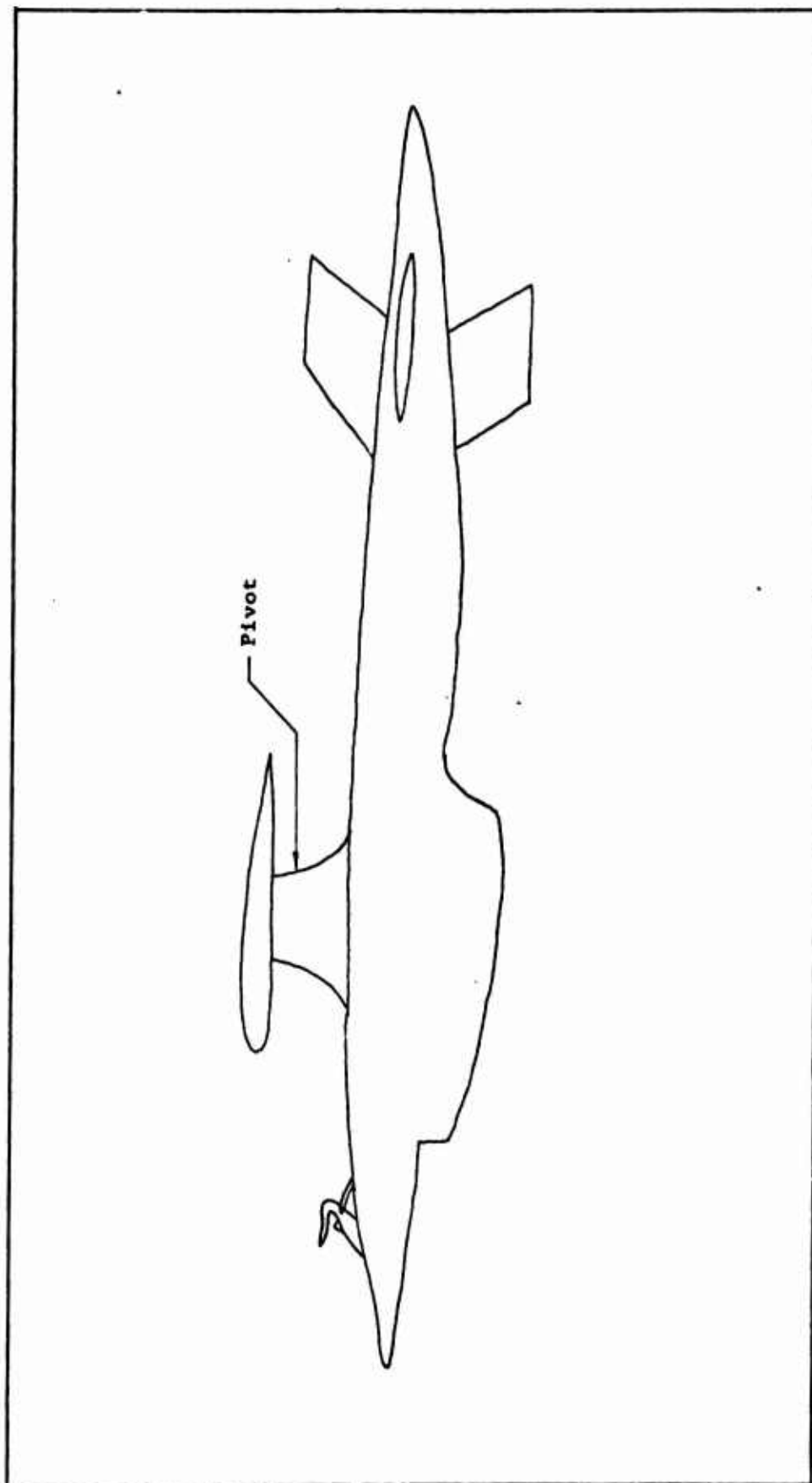


Figure 1. Oblique-Winged RPV

fly at various Mach numbers while performing its mission. With the RPV locked to the mothership by the supports, the wing can be pivoted to decrease the span for storage inside the mothership fuselage.

Capture System

Potential in-flight capture systems can be based on the following approaches: a. launch and recovery of the RPV from the wing of the mothership with external carry, b. launch and recovery of the RPV from the tail of the mothership with external carry, and c. launch and recovery of the RPV from the fuselage of the mothership with internal carry. The latter approach is the basis for the concepts presented in this thesis.

The capture system is divided into the trapeze (carried on the mothership aircraft) and the skyhook (carried on the RPV). The terms trapeze and skyhook were used in the XP-85 project and are carried over by this author. Two capture systems are considered in this thesis. The first system involves recovery through bomb bay doors in the fuselage (Fig. 2, p. 7). The second system involves recovery through a tail door (Fig. 3, p. 8). In both capture systems the RPV flies from the rear toward the mothership. During the capture sequence, the RPV approaches the trapeze (docking point) with the skyhook extended. As the RPV closes on the trapeze the closing rate is reduced. The skyhook is guided into the capture bar by two arms (see Fig. 6, p. 13). Once the RPV locks on to the bar the engine thrust is reduced and the RPV is then towed. While the RPV is in tow, the aft support is lowered and locked in place to stabilize the RPV for raising into the mothership for storage. Once the aft supports are secured the engine is shut off.

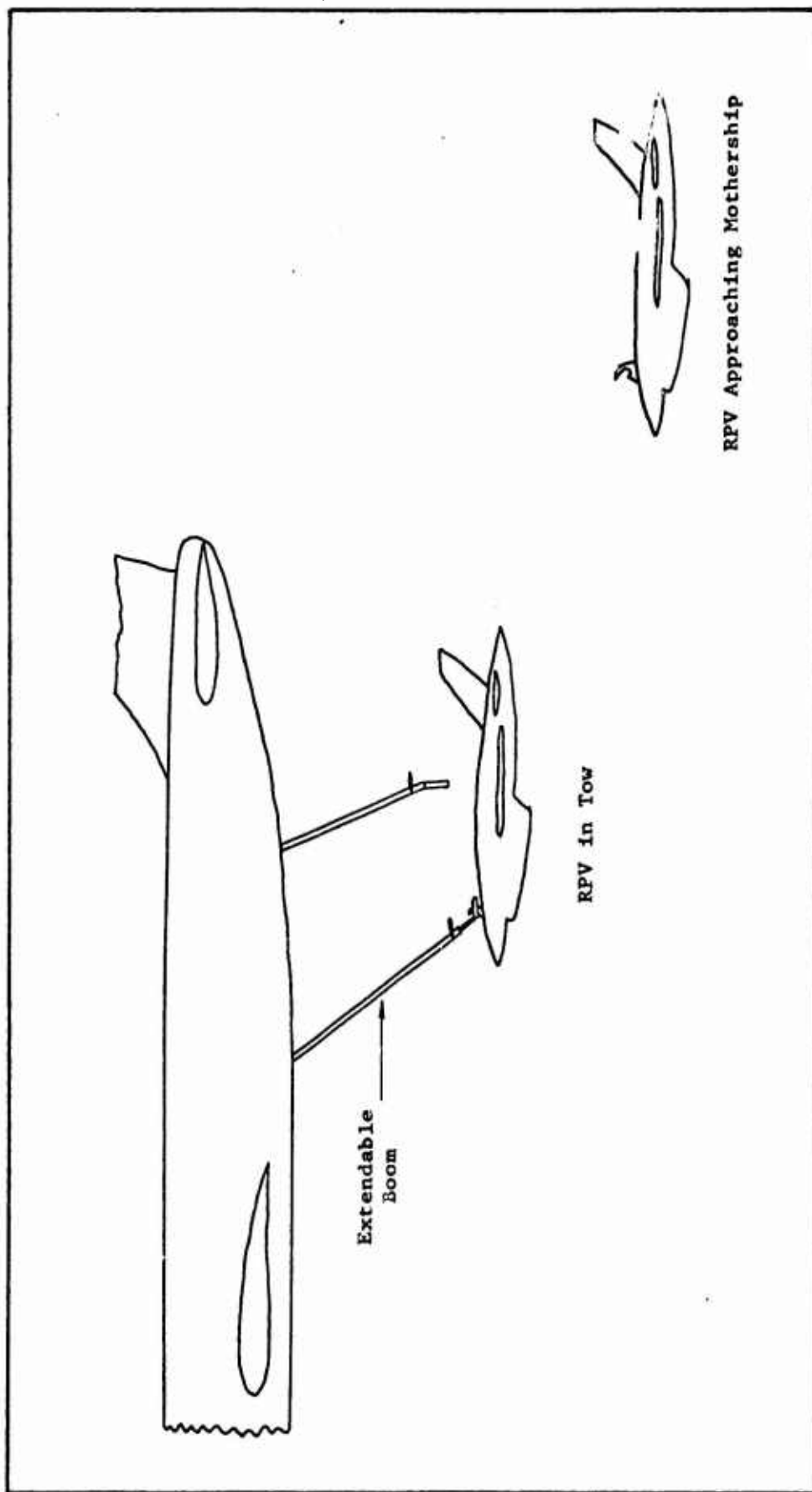


Figure 2. RPV Capture System (Bomb Bay Doors)

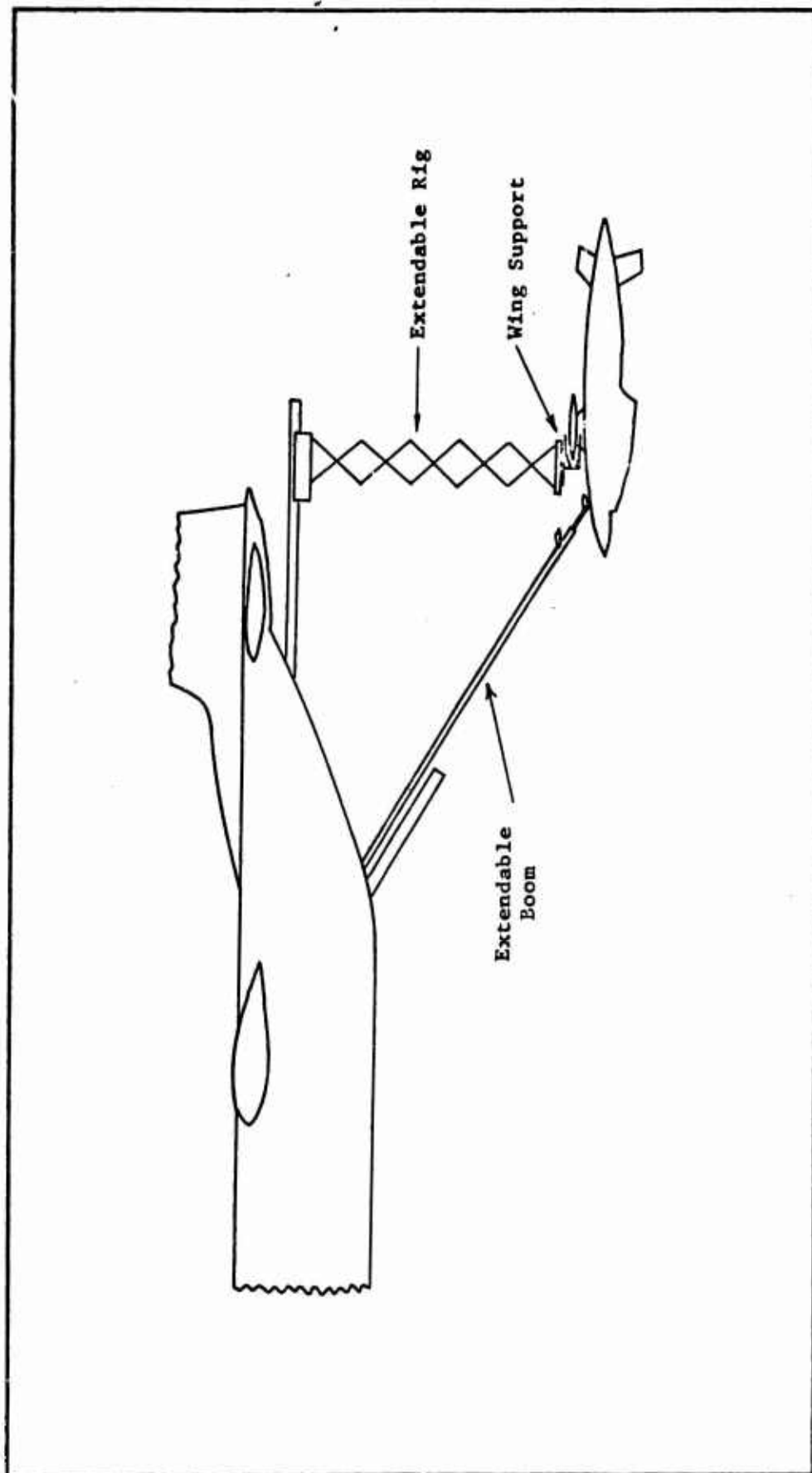


Figure 3. RPV Capture System (Aft Doors)

The skyhook and the associated trapeze is the same for both capture systems (see Skyhook, p. 9 and Trapeze, p. 12). The aft support used with the bomb bay doors is shown in Fig. 6 , p. 13 . The wing support used with the tail door is shown in Fig. 7, p. 14 .

Skyhook. The skyhook for the XP-85 was located 2 to 7 inches ahead of and above the center of gravity of the aircraft. During the flight testing of the XP-85, with a trapeze attached to a B-29, McDonnell Aircraft Corporation found that this position was unsuitable because the XP-85 became marginally stable, directionally, while attached to the trapeze. McDonnell recommended that any future designs should locate the skyhook well ahead of the center of gravity so that the aircraft is towed after attachment to the trapeze (Ref 2:10). The XF-84F which followed the XP-85 had the skyhook located close to the nose of the aircraft (Ref 3: A3). Based on the information gained from the XP-85 and XF-84F projects, the skyhook should be located on the nose of the RPV as shown in Fig. 4, p. 10 . The exact location of the skyhook must be determined by an analysis of the RPV stability while attached to the trapeze.

The skyhook design concepts presented are similar to the design used in the XF-84F project. The skyhook design is common to both capture systems. The skyhook (see Fig. 5, p. 11) consists of a hook rigidly attached to the RPV at its base and free to rotate in the plane of symmetry of the RPV. The hook is raised and lowered by a shock absorbing shaft attached to a slide. The slide travels along a track which is fixed to the RPV. When the skyhook is completely extended the slide is locked in place for docking. The shock absorbing shaft is used to absorb some of the energy that must be dissipated during docking.

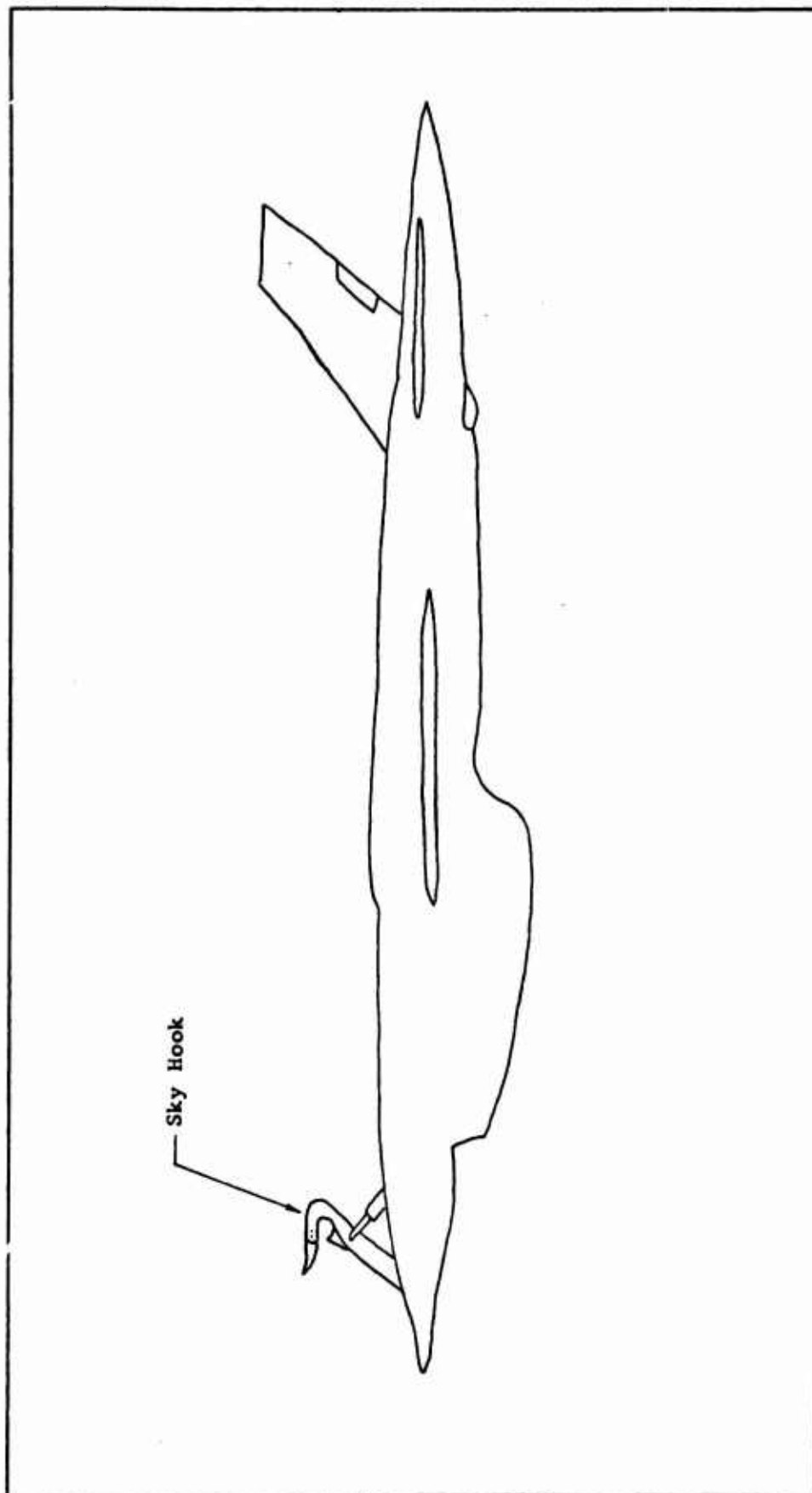


Figure 4. Fixed-Wing RPV with Skyhook Extended

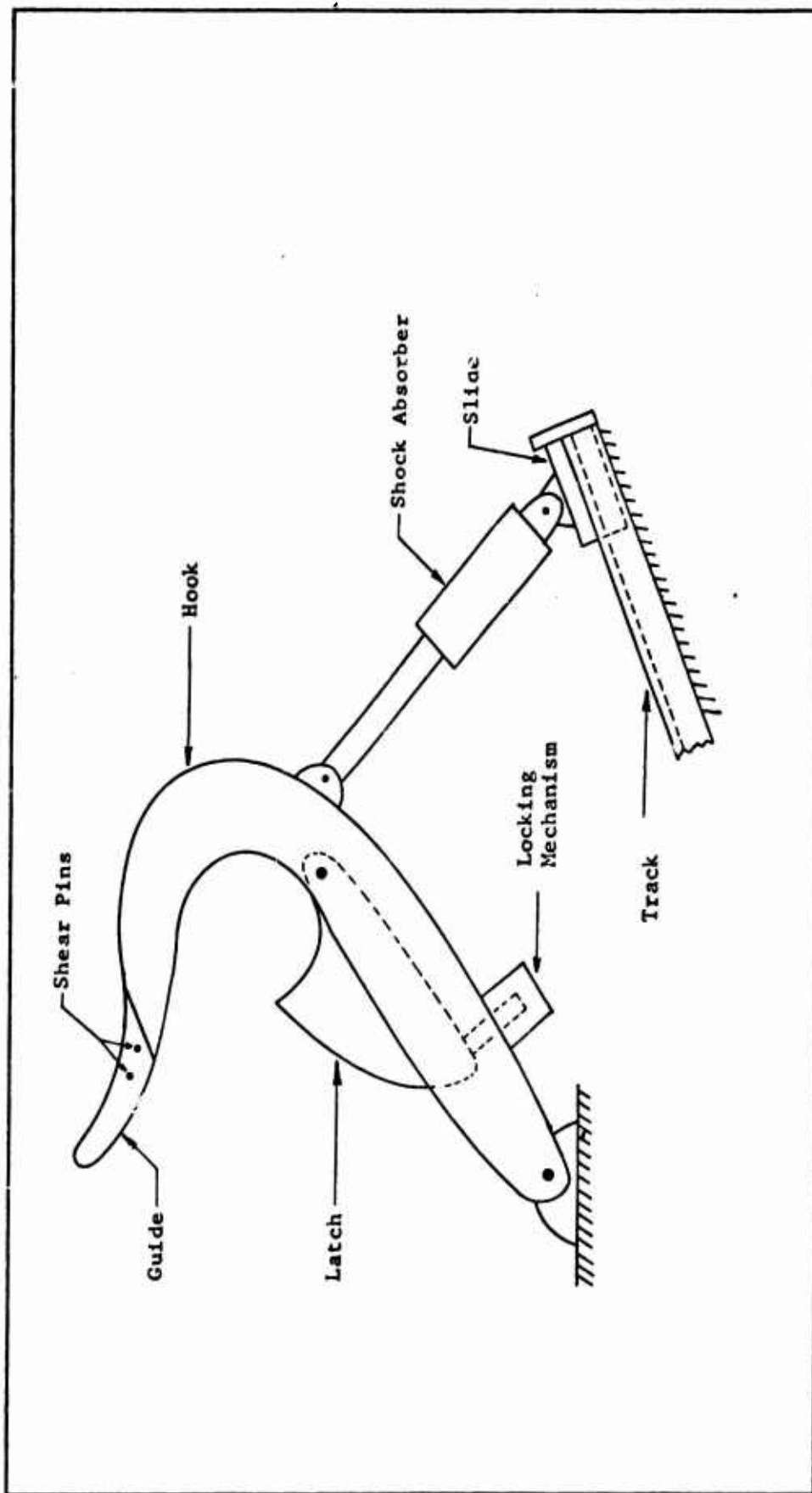


Figure 5. Skyhook

In the hook is a latch which locks onto the docking bar of the trapeze. At the end of the hook a guide is attached by shear pins to increase the contact area with the attachment bar of the trapeze.

Trapeze. During docking the skyhook locks onto the trapeze attachment bar. The trapeze puts the RPV in tow by the mothership.

The trapeze is a extendable shaft, similar to the KC-135 refueling boom, with a docking head on the end (Fig. 6, p. 13 and Fig. 7, p. 14) and is common to both capture systems. The docking head should be at least two fuselage diameters of the mothership below the fuselage. This length was suggested as a result of the flight tests of the XF-85 project (Ref 2: 10) which indicated that the distance was outside the turbulent boundary layer. Located above the docking head are two moveable guide wings for controlling the trapeze.

The docking head is attached to the tow boom by a pivot which will allow the docking head to swing in the plane of symmetry of the mothership. A shock absorber is attached at one end to the tow boom and at the other end to the docking head. The shock absorber is used to hold the docking head vertical and to absorb some of the energy of the RPV hook up with the docking head.

The docking head is a fork with the two prongs pointed vertically downward, away from the mothership. Joining the tips of the prongs is the attachment bar. Guides are attached to the tips of the prongs to increase the contact area and guide the skyhook to the attachment bar.

With the skyhook locked on to the attachment bar of the trapeze the thrust is reduced. While the RPV is being towed, the aft support is lowered. Each of the aft supports is discussed separately.

Aft Support, Fixed Wing RPV. The aft support is designed to provide

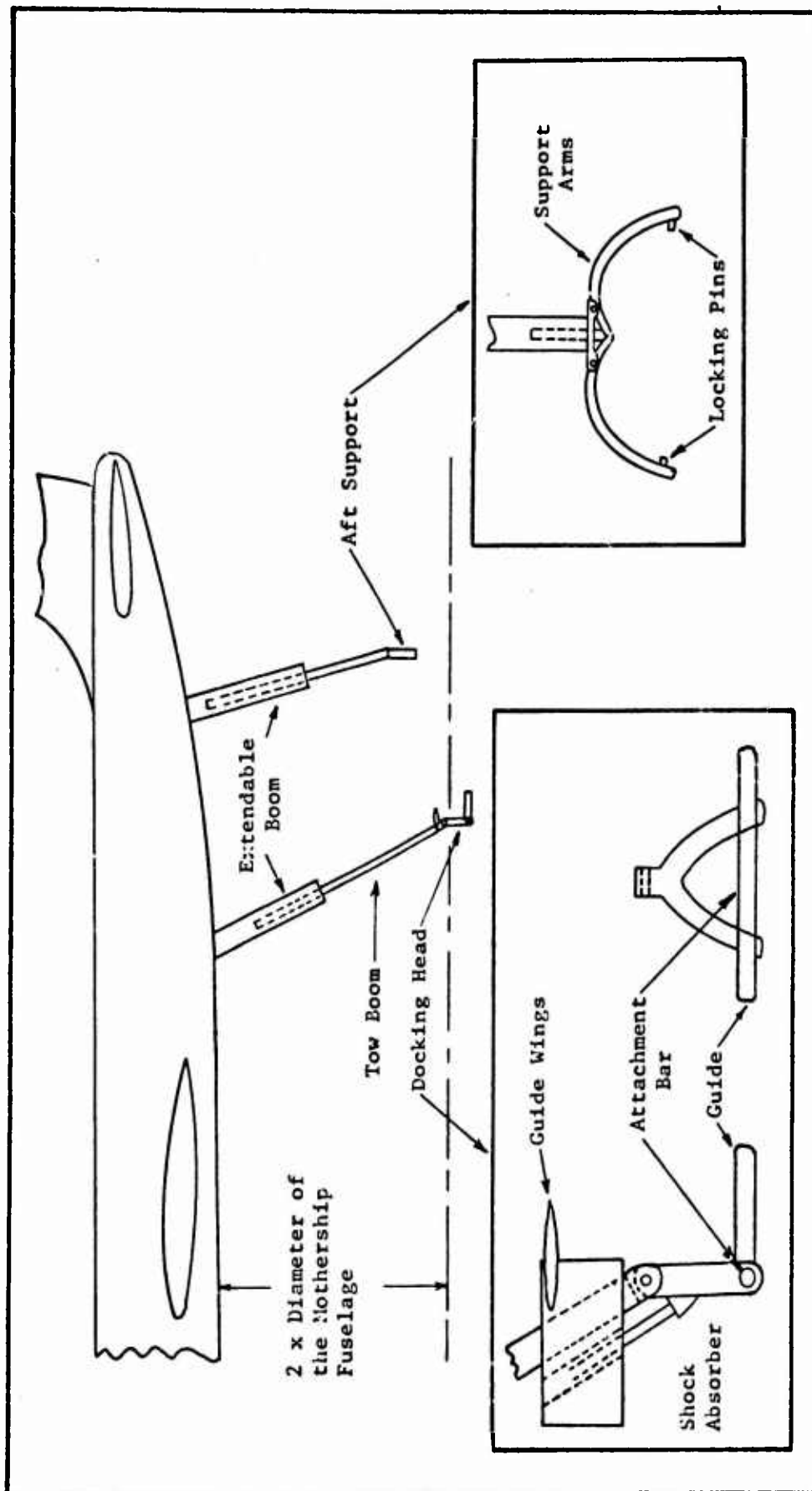


Figure 6. Bomb Bay Trapeze

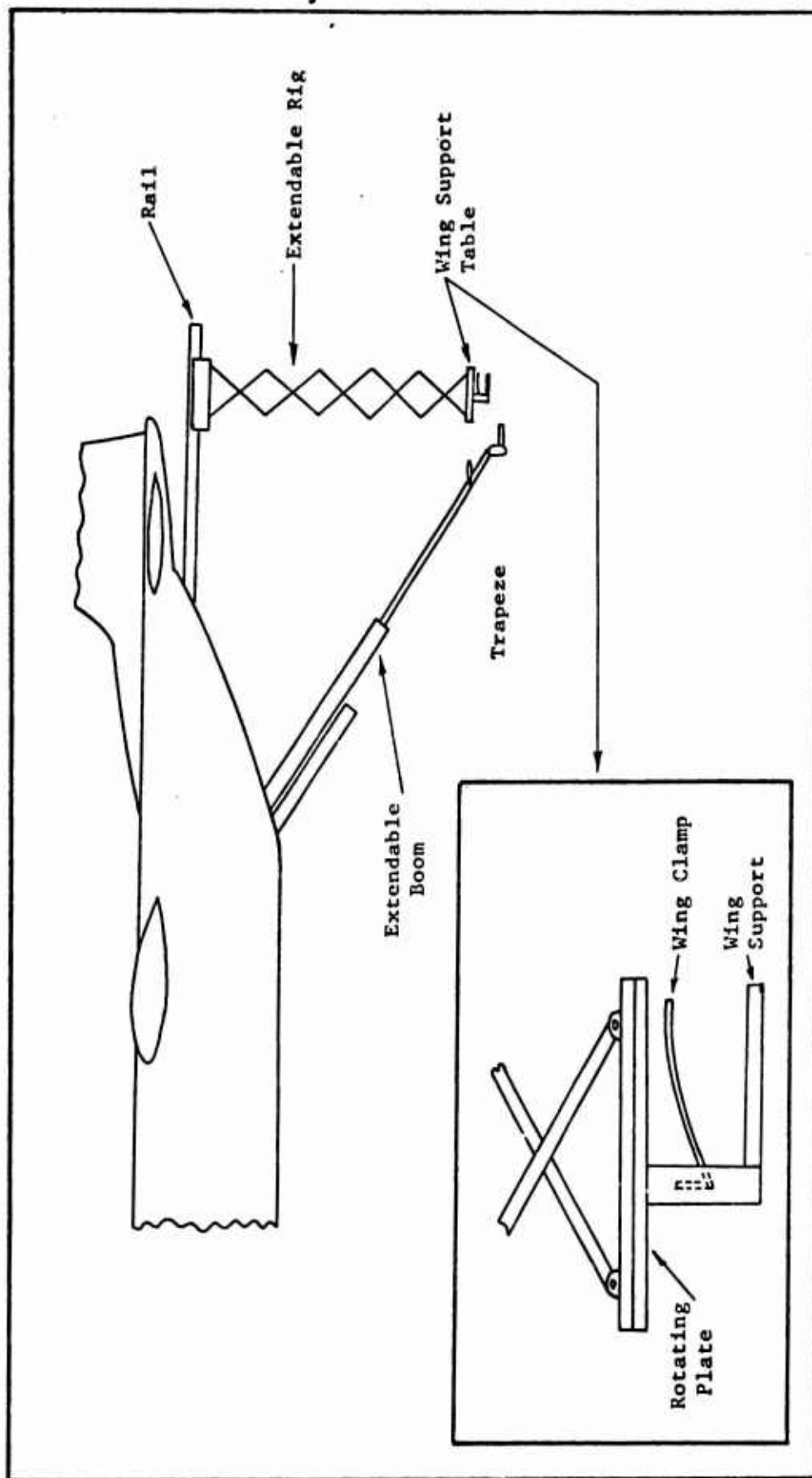


Figure 7. Aft Door Trapeze

pitch and directional stability during the storage sequence. The aft support contacts the fixed wing RPV on the fuselage behind the center of gravity. Fig. 6, p. 13 shows a schematic drawing of the aft support. The aft support is located at the end of an extendable boom like the docking head. A set of claw like arms are used to encircle the aft part of the fuselage and lock in place.

Aft Support, Oblique Wing RPV. For the oblique-wing RPV proposed in this thesis a different aft support may be used. The aft support shown schematically in Fig. 7, p. 14, is a wing support. The extendable rig moves on a rail attached to the mothership. When the RPV is in tow, the wing support table is lowered in front of the RPV wing and then moved back to enclose the wing on both sides of the pivot. The wing clamp is then locked in place for raising into the fuselage. For storage the wing support table and wing are rotated so that the wing is parallel to the fuselage.

III. Horseshoe Vortex Model of Mothership

In this thesis the mothership is modeled by an elliptical distribution of horseshoe vortex elements on the mothership wing. The induced velocity on the RPV during the capture sequence was obtained from the horseshoe vortex model. Because the RPV was assumed to be much smaller than the mothership, the effect of the RPV on the mothership velocity environment was assumed to be negligible. Figure 8, p.17, shows the coordinate system and the relationships used in the horseshoe vortex model of the mothership. The induced velocity at point (X_1, Y_1, Z_1) , where point P represents the location of the RPV wing from the origin in the mothership, is obtained using the Biot-Savart Law. The total induced velocity q at the point P can be obtained by summing the individual contributions of the bound vortex and each of the two trailing vortex filaments.

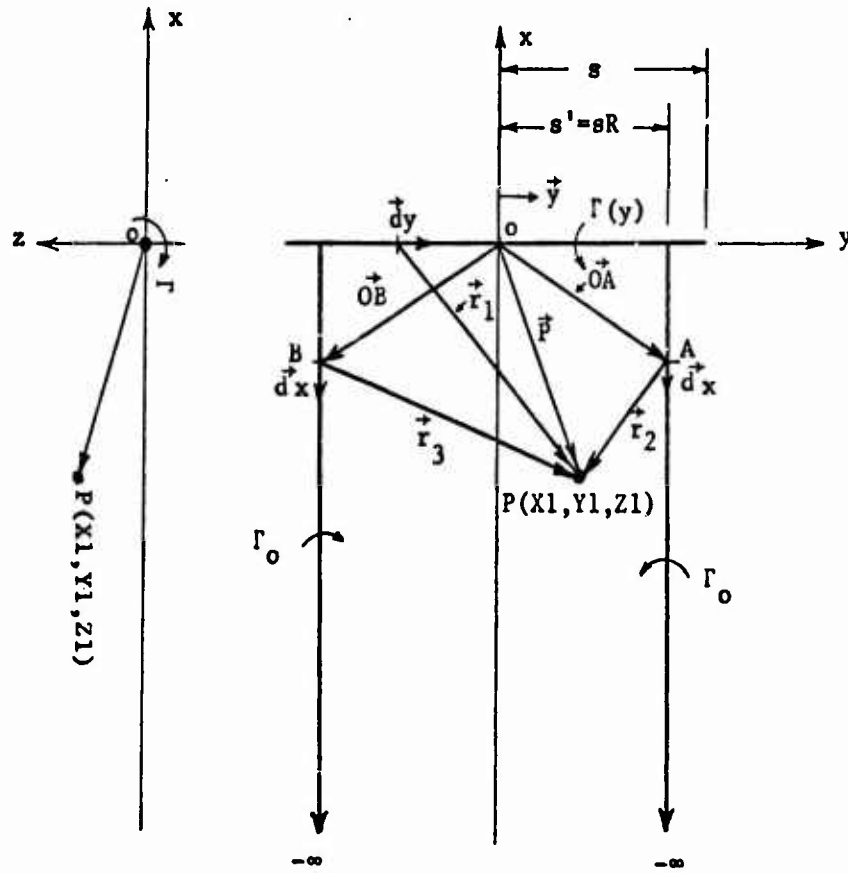
As an initial step in formulating the mothership model, an elliptical spanwise distribution of lift of the mothership wing was assumed. Glauert justifies this assumption by the following statements taken from his book (Ref 4:143).

"The elliptic distribution of circulation or lift across the span of an aerofoil is important, firstly because it leads to the minimum possible induced drag for a given total lift, and secondly because the load grading curves of most aerofoils of conventional shape do not differ greatly from the elliptic form. The results deduced from the hypothesis of elliptic loading are therefore the best which can possibly occur and are also a good first approximation to those actually obtained".

The mothership was modeled by the wing only, no fuselage or tail effects were considered in the model. The wing was assumed to be straight

Side View

Top View



Vector Relationships

$$d\vec{x} = -dx \hat{i}$$

$$d\vec{y} = dy \hat{j}$$

$$\vec{r}_1 = (\vec{p} - \vec{y}) = X1 \hat{i} + (Y1 - y) \hat{j} + Z1 \hat{k}$$

$$\vec{r}_2 = (\vec{p} - \vec{OA}) = (X1 - x) \hat{i} + (Y1 - sR) \hat{j} + Z1 \hat{k}$$

$$\vec{r}_3 = (\vec{p} - \vec{OB}) = (X1 - x) \hat{i} + (Y1 + sR) \hat{j} + Z1 \hat{k}$$

NOTE: The sign of the symbols used in the vector expressions are positive except for sR . Thus the value of the symbol to be substituted into the above expression carries a sign.

Figure 8. Mothership Horseshoe Vortex

with an elliptic distribution of lift across the span. The elliptic distribution of lift (elliptic loading) is proportional to the circulation around the airfoil. The wing with a steady flow of air passing over it can be represented by individual vortex lines which combine linearly to produce the elliptic distribution of circulation around the airfoil. These individual vortex lines consist of bound vortex segments, representing the wing itself, and free vortex lines that trail from the wings trailing edge. The trailing vortex lines form a trailing vortex sheet behind the wing. When the starting vortex is infinitely down stream, the vortex lines form what is called a horseshoe vortex.

The sheet of trailing vortex lines is unstable, so downstream of the airfoil the vortex sheet rolls up into two trailing vortex lines which have strength equal to the sum of the individual vortex filaments that make up the trailing vortex sheet. For an elliptically loaded wing the sum of the individual horseshoe vortex filaments is a maximum at mid-span with a value of Γ_0 and decreases elliptically to zero at the wing tips. The trailing vortices then have a constant strength of Γ_0 . The centers of the trailing vortices, for an elliptically loaded wing, are shown by Milne-Thomson (Ref 5:206) to be separated by a distance equal to $\pi/4$ times the wing span.

Treating the wing as a horseshoe vortex to study the effects away from the wing itself is stated by Houghton and Brock (Ref 6:336) to give good results at distances greater than two chord lengths from the center of pressure of the wing. The effect of the mothership, modeled by the horseshoe vortex, is found by first determining the induced velocity contribution from the bound vortex, and then finding the induced velocity contribution from each of the trailing vortices.

Contribution of Bound Vortex

The bound vortex lies along the y-axis with a length $2s$, where s is the semi-span of the mothership wing. The bound vortex induced velocity at point P is called \vec{q}_1 . For the elliptically loaded airfoil the distribution of circulation across the span is

$$\Gamma(y) = \frac{\Gamma_0}{s} \sqrt{s^2 - y^2} \quad (1)$$

where Γ_0 is the maximum circulation at the midsection of the wing (Ref 7:548). The value of Γ_0 is given by

$$\Gamma_0 = \frac{2L}{\pi \rho V_\infty S} = \frac{2W}{\pi \rho V_\infty S} \quad (2)$$

(Ref 7:550).

The induced velocity \vec{q}_1 at point P is then given by the Biot-Savart Law as

$$\vec{V}(\vec{r}_1) = \frac{1}{4\pi} \int_{-s}^s \frac{\Gamma(y)(d\vec{y} \times \vec{r}_1)}{|\vec{r}_1|^3} \quad (\text{cross product}) \quad (3)$$

(Ref 7:528).

Substituting in the expression for $\Gamma(y)$ the induced velocity \vec{q}_1 is

$$\vec{q}_1 = \frac{\Gamma_0}{4\pi s} \int_{-s}^s \frac{\sqrt{s^2 - y^2}(d\vec{y} \times \vec{r}_1)}{|\vec{r}_1|^3} \quad (4)$$

As shown in Fig. 8, p. 18,

$$\vec{r}_1 = (\vec{P} - \vec{y}) = X1 \hat{i} + (Y1 - y) \hat{j} + Z1 \hat{k} \quad (5)$$

and $d\vec{y} = dy \hat{j}$. Evaluating the cross product $d\vec{y} \times \vec{r}_1$ gives

$$d\vec{y} \times \vec{r}_1 = Z1 dy \hat{i} - X1 dy \hat{k}. \quad (6)$$

Also, $|\vec{r}_1| = \sqrt{X1^2 + (Y1 - y)^2 + Z1^2}$. Substituting these expressions into

the equation for \vec{q}_1 gives

$$\vec{q}_1 = \frac{\Gamma_0}{4\pi s} \int_{-s}^s \frac{(s^2 - y^2)^{\frac{1}{2}} (Z_1 dy \hat{i} - X_1 dy \hat{k})}{(X_1^2 + (Y_1 - y)^2 + Z_1^2)^{3/2}} \quad (7)$$

The expression is now factored into the two components

$$q_{1x} \hat{i} = \frac{\Gamma_0 Z_1}{4\pi s} \int_{-s}^s \frac{(s^2 - y^2)^{\frac{1}{2}} dy}{(X_1^2 + (Y_1 - y)^2 + Z_1^2)^{3/2}} \hat{i} \quad (8)$$

and

$$q_{1z} \hat{k} = - \frac{\Gamma_0 X_1}{4\pi s} \int_{-s}^s \frac{(s^2 - y^2)^{\frac{1}{2}} dy}{(X_1^2 + (Y_1 - y)^2 + Z_1^2)^{3/2}} \hat{k} \quad (9)$$

Contribution from Trailing Vortices

The trailing vortex sheet formed by the distribution of individual horseshoe vortices across the wing is unstable at the wing tips and rolls up into two trailing vortex filaments. The single trailing vortex filaments that result from the vortex sheet rolling up, start at points set back from the wing tips. The distance the trailing vortex is off set from the wing tip is a distance $(s - s')$ where s is the wing semi-span and s' is the semi-span of the trailing vortex filaments. The two semi-spans s and s' can be related by the ratio $R = s'/s$. For an elliptically loaded wing Glauert gives a ratio of $s'/s = \frac{\pi}{4}$ (Ref 4:168). The strength of each trailing vortex filament is the sum of each element in the sheet and is equal to the circulation around the center of the wing, that is Γ_0 .

Using the Biot-Savart Law with the circulation constant at Γ_0 the induced velocity from the $+s'$ trailing vortex and the $-s'$ trailing vortex are \vec{q}_2 and \vec{q}_3 , respectively. To calculate \vec{q}_2 and \vec{q}_3 the notation of Fig. 8, p. 17 is used.

Calculation of \vec{q}_2 . Beginning with the Biot-Savart Law for a semi-infinite vortex filament starting at $+s'$, the induced velocity \vec{q}_2 at point P is

$$\vec{q}_2(P) = \frac{\Gamma_0}{4\pi} \int_0^{-\infty} \frac{(\vec{dx} \times \vec{r}_2)}{|\vec{r}_2|^3} \quad (10)$$

where $\vec{dx} = +dx \hat{i}$ (dx points in the direction of integration and is a negative increment in the integration.)

$$\vec{r}_2 = (X1 - x) \hat{i} + (Y1 - sR) \hat{j} + Z1 \hat{k}, \quad (11)$$

$$\text{and } |\vec{r}_2| = \sqrt{(X1 - x)^2 + (Y1 - sR)^2 + Z1^2}$$

Evaluation of the cross-product gives $\vec{dx} \times \vec{r}_2 = -Z1 dx \hat{j} + (Y1 - sR) dx \hat{k}$. Substituting these into the integral equation for $\vec{q}_2(P)$ the following is obtained.

$$\vec{q}_2(P) = \frac{-\Gamma_0}{4\pi} \int_0^{-\infty} \frac{Z1 dx \hat{j} - (Y1 - sR) dx \hat{k}}{[(X1 - x)^2 + (Y1 - sR)^2 + Z1^2]^{3/2}} \quad (12)$$

This equation is broken into the components and integrated.

To integrate the equation for $\vec{q}_2(P)$ the denominator is expanded to

$$x^2 - 2 X1 x + X1^2 + (Y1 - sR)^2 + Z1^2 \quad (13)$$

Letting

$$\begin{aligned} a &= X1^2 + (Y1 - sR)^2 + Z1^2 \\ b &= -2 X1 \\ c &= 1 \end{aligned} \quad (14)$$

and using integral formula No. 184 from Ref 8:297;

$$\int \frac{dx}{X\sqrt{X}} = \frac{2(2cx + b)}{q\sqrt{X}} \quad (15)$$

where $X = a + bx + cx^2$

$$q = 4ac - b^2$$

the following expression is obtained for $q_{2y}(P) \hat{j}$.

$$q_{2y}(P) \hat{j} = \frac{-\Gamma_0 Z_1}{4\pi} \frac{2(2x - 2X_1)}{[4(X_1^2 + (Y_1 - sR)^2 + Z_1^2) - 4X_1^2][(x - X_1)^2 + (Y_1 - sR)^2 + Z_1^2]^{\frac{1}{2}}} \int_0^{\infty} \hat{j} \quad (16)$$

This equation can be reduced by algebraic manipulation to

$$q_{2y}(P) \hat{j} = \frac{-\Gamma_0 Z_1}{4\pi[(Y_1 - sR)^2 + Z_1^2]} \left[\frac{(x - X_1)}{[(x - X_1)^2 + (Y_1 - sR)^2 + Z_1^2]^{\frac{1}{2}}} \right] \int_0^{\infty} \hat{j} \quad (17)$$

This improper integral is evaluated at the end points, using only the bracketed quantity.

$$\lim_{x \rightarrow \infty} \left[\frac{(x - X_1)}{[(x - X_1)^2 + (Y_1 - sR)^2 + Z_1^2]^{\frac{1}{2}}} \right] - \frac{-X_1}{[X_1^2 + (Y_1 - sR)^2 + Z_1^2]^{\frac{1}{2}}} \quad (18)$$

Dividing both numerator and denominator of the limit quantity by $+(x - X_1)$ which leaves -1 because the quantity is negative as $x \rightarrow \infty$, the limit is

$$\lim_{x \rightarrow \infty} \left[\frac{-1}{\left[1 + \frac{(Y_1 - sR)^2}{(x - X_1)^2} + \frac{Z_1^2}{(x - X_1)^2} \right]^{\frac{1}{2}}} \right] = -1 \quad (19)$$

Combining the parts of the equation, the y-component of the induced velocity is thus

$$q_{2y}(P) \hat{j} = \frac{+\Gamma_0 Z_1}{4\pi[(Y_1 - sR)^2 + Z_1^2]} \left[1 - \frac{X_1}{[X_1^2 + (Y_1 - sR)^2 + Z_1^2]^{\frac{1}{2}}} \right] \hat{j} \quad (20)$$

Identical evaluation for the z-component gives,

$$q_{2z}(P) \hat{k} = - \frac{\Gamma_0 (Y_1 - sR)}{4\pi[(Y_1 - sR)^2 + Z_1^2]} \left[1 - \frac{X_1}{[X_1^2 + (Y_1 - sR)^2 + Z_1^2]^{\frac{1}{2}}} \right] \hat{k} \quad (21)$$

Calculation of \vec{q}_3 . Again, using the Biot-Savart Law to calculate \vec{q}_3 for a semi-infinite vortex filament starting at $-s'$ the following is obtained. Γ_0 has a negative sign in this development because its direction

is opposite to that for \vec{q}_2 . The induced velocity \vec{q}_3 is thus

$$\vec{q}_3(P) = \frac{-\Gamma_0}{4\pi} \int_0^{-\infty} \frac{(\vec{dx} \times \vec{r}_3)}{|\vec{r}_3|^3} \quad (22)$$

where $\vec{dx} = dx \hat{i}$ (Again, dx is a negative increment in the integration)

$$\vec{r}_3 = (X1 - x) \hat{i} + (Y1 + sR) \hat{j} + Z1 \hat{k}$$

$$\text{and } |\vec{r}_3| = (X1 - x)^2 + (Y1 + sR)^2 + Z1^2$$

Evaluation of the cross-product gives $\vec{dx} \times \vec{r}_3 = Z1 dx \hat{j} + (Y1 + sR) dx \hat{k}$.

Substituting into the integral gives

$$\vec{q}_3(P) = \frac{+\Gamma_0}{4\pi} \int_0^{-\infty} \frac{Z1 dx \hat{j} - (Y1+sR) dx \hat{k}}{[(X1-x)^2 + (Y1+sR)^2 + Z1^2]^{3/2}} \quad (23)$$

Evaluation of the integral is identical to that for $\vec{q}_2(P)$ and the result

in component form is:

y-component:

$$q_{3y}(P) \hat{j} = \frac{-\Gamma_0 Z1}{4\pi[(Y1+sR)^2 + Z1^2]} \left[1 - \frac{X1}{[X1^2 + (Y1+sR)^2 + Z1^2]^{1/2}} \right] \hat{j} \quad (24)$$

z-component:

$$q_{3z}(P) \hat{k} = \frac{+\Gamma_0(Y1+sR)}{4\pi[(Y1+sR)^2 + Z1^2]} \left[1 - \frac{X1}{[X1^2 + (Y1+sR)^2 + Z1^2]^{1/2}} \right] \hat{k} \quad (25)$$

Total Induced Velocity

In summary, the total induced velocity at the point P is the vector sum of the induced velocities created by the bound vortex filament and each of the two trailing vortex filaments, that is $\vec{q}(P) = \vec{q}_1(P) + \vec{q}_2(P) + \vec{q}_3(P)$. The total velocity at point P is the vector sum of the induced velocity $\vec{q}(P)$ and the free stream velocity $\vec{U}_\infty = u_\infty \hat{i} + v_\infty \hat{j} + w_\infty \hat{k}$. If the free stream velocity is directed along the negative x-axis then $\vec{U}_\infty = -U_\infty \hat{i}$ and the relative velocity at the point P is $\vec{U}_\infty + \vec{q}(P)$. In component form the relative velocity at the point P is:

x-component: $u(P) \hat{i} = -U_{\infty} \hat{i} + q_1(P) \hat{i}$

$$u(P) = -U_{\infty} + \frac{\Gamma_0 P_3}{4\pi s} \int_{-s}^s \frac{(s^2 - y^2)^{\frac{1}{2}} dy}{[X1^2 + (Y1 - y)^2 + Z1^2]^{3/2}} \quad (26)$$

y-component: $v(P) \hat{j} = q_{2_y}(P) \hat{j} + q_{3_y}(P) \hat{j}$

$$v(P) = \frac{+\Gamma_0 Z1}{4\pi[(Y1-sR)^2 + Z1^2]} \left[1 - \frac{X1}{[X1^2 + (Y1-sR)^2 + Z1^2]^{1/2}} \right] - \frac{\Gamma_0 Z1}{4\pi[(Y1+sR)^2 + Z1^2]} \left[1 - \frac{X1}{[X1^2 + (Y1+sR)^2 + Z1^2]^{1/2}} \right] \quad (27)$$

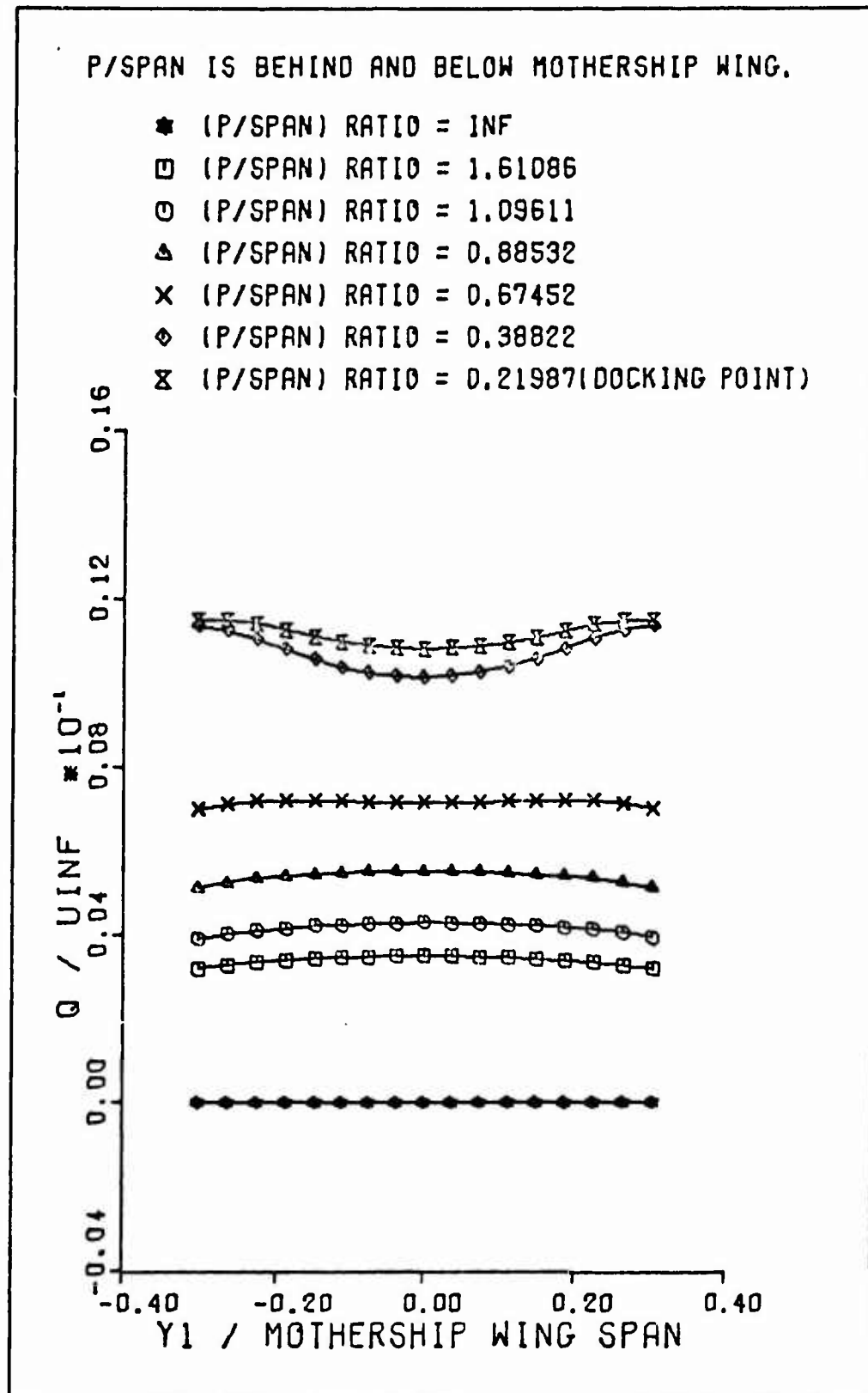
z-component: $w(P) \hat{k} = q_{1_z}(P) \hat{k} + q_{2_z}(P) \hat{k} + q_{3_z}(P) \hat{k}$

$$w(P) = -\frac{\Gamma_0 X1}{4\pi s} \int_{-s}^s \frac{(s^2 - y^2)^{\frac{1}{2}} dy}{[X1^2 + (Y1 - y)^2 + Z1^2]^{3/2}} - \frac{\Gamma_0 (Y1-sR)}{4\pi[(Y1-sR)^2 + Z1^2]} \left[1 - \frac{X1}{[X1^2 + (Y1-sR)^2 + Z1^2]^{1/2}} \right] + \frac{\Gamma_0 (Y1+sR)}{4\pi[(Y1+sR)^2 + Z1^2]} \left[1 - \frac{X1}{[X1^2 + (Y1+sR)^2 + Z1^2]^{1/2}} \right] \quad (28)$$

Analysis of Induced Velocity

A computer program was written to calculate the relative velocity of point P as the point was moved relative to the horseshoe vortex. Appendix A contains the computer program which was used to calculate the induced velocity from the equations presented in the preceeding section. The induced velocity $\vec{q}(P)$ generated by the horseshoe vortex model is plotted in Fig. 9, p. 25, for $U_{\infty} = 300.0$ knots and in Fig. 10, p. 26, for $U_{\infty} = 200.0$ knots.

The variation of induced velocity plots were generated by fixing a value of X1, Z1 and then computing the induced velocity for the range of

Figure 9. Induced Velocity Distribution, $U_{\infty} = 300$ Knots

P/SPAN IS BEHIND AND BELOW MOTHERSHIP WING.

- * (P/SPAN) RATIO = INF
- (P/SPAN) RATIO = 1.61086
- (P/SPAN) RATIO = 1.09611
- △ (P/SPAN) RATIO = 0.88532
- x (P/SPAN) RATIO = 0.67452
- ◇ (P/SPAN) RATIO = 0.38822
- ⊗ (P/SPAN) RATIO = 0.21987 (DOCKING POINT)

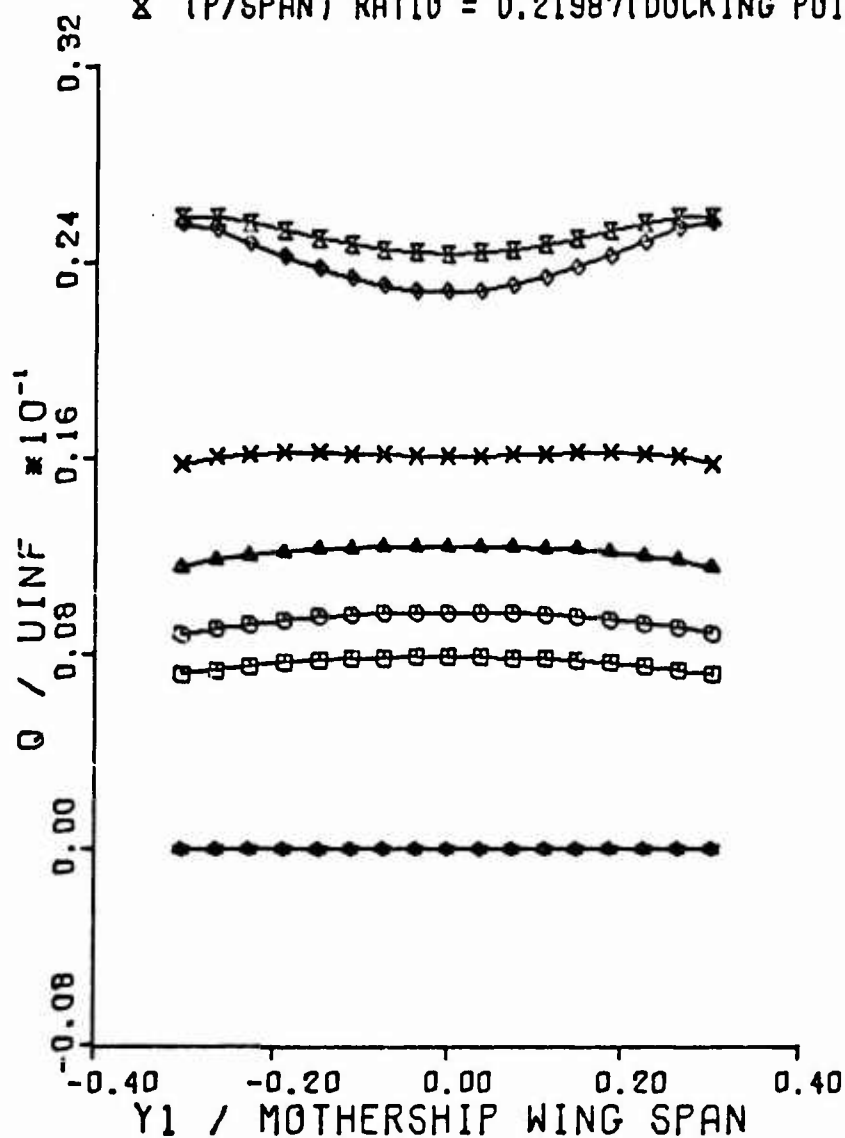


Figure 10. Induced Velocity Distribution, $U_{\infty} = 200$ Knots

values of Y_1 shown. The induced velocity was non-dimensionalized by the free stream velocity and the distance Y_1 from the plane of symmetry of the mothership was non-dimensionalized with the mothership wing span.

The plots of non-dimensional induced velocity verse non-dimensional Y_1 show a variation in curvature. The variation in curvature of the velocity was caused by the variation in the effect of the u , v , and w components of induced velocity. The u -component comes only from the elliptic distribution of circulation on the bound vortex. The v -component comes only from the trailing vortices but as X_1 increases in negative value, the fraction $X_1 / [X_1^2 + (Y_1 \pm sR)^2 + Z_1^2]^{1/2}$ increases in negative value. The fraction is subtracted from 1 thus reducing the v -component for fixed values of Y_1 . Conversely as the negative value of X_1 approaches zero the fraction becomes a progressively smaller negative number which is subtracted from 1 thus increasing the v -component. For fixed values of X_1 , Z_1 the v -component of induced velocity increases as the trailing vortex is approached. The w -component of induced velocity comes from both the bound vortex and the trailing vortices. The merging of the plots for $P/\text{span} = 0.38822$ and 0.21987 , at values of $Y_1/\text{mothership wing span}$ greater than ± 0.20 is the result of the v and w components magnitude dominating the u components magnitude.

At values of $P/\text{span} = 0.67452$ and greater the relatively flat velocity variation for increasing values of Y_1 supports the assumption of constant velocity across the RPV span. But as shown in both velocity plots this assumption breaks down as the docking point is approached. Variation of velocity across the RPV span becomes important if the RPV is out of the plane of symmetry close to the docking point.

The induced velocity generated at $U_\infty = -200.0$ knots is greater than

for $U_{\infty} = 300.0$ knots. The increase in induced velocity as U_{∞} is decreased is caused by the circulation, computed from equation 2 , p. 19 , increasing as velocity decreases.

IV. Steady State Analysis of Aerodynamic Interference

The flow field seen by the RPV during approach to the docking point was modeled by replacing the mothership with a horseshoe vortex as previously described. It was shown in the section Analysis of Induced Velocity, p. 24, that the flow field is essentially constant across the RPV wing span when the RPV flight path is within a distance of ± 0.1 of the mothership wing span from the mothership plane of symmetry. In analyzing the aerodynamic interference of the mothership on the RPV it was assumed that the RPV flight path remained in the plane of symmetry of the mothership.

In the analysis it was assumed that both the mothership and the RPV were flying steadily through a stationary atmosphere (no wind). A transformation was made to bring the aircraft to rest and give the air a negative velocity equal in magnitude and opposite in direction to the flight velocity.

The mothership effects a change in the velocity vector seen by the RPV. Both the magnitude and direction of the velocity vector are changed. To show the effect of the changed velocity vector the RPV lift, lift induced drag, and aerodynamic pitching moment were computed as the RPV approached, the docking point. In the analysis, all values were calculated using the RPV parameters at the plane of symmetry as representative.

The approach to the docking point that was found to be best during the flight tests of the XF-85 is shown in Fig. 11, p. 30 (Ref 9:46-49). The first segment of the flight path was level, about 5 times the diameter of the mothership below the docking point. A gradual increase in RPV altitude was then made to bring the RPV to a point approximately one mothership wing mean aerodynamic chord behind and level with the docking

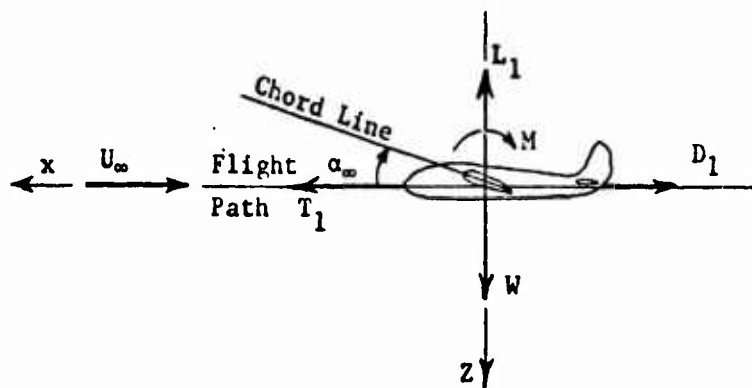
point. The RPV was then flown level into the docking point at a low closing velocity (less than 5 knots). For the analysis the RPV approached the docking point along a level flight path ($\theta = 0^\circ$ in Fig. 11). A level flight path was chosen to remove the effects of climb which produced discontinuities in the data at the points where the flight path changed direction.

A hypothetical RPV was used in analyzing the variation of the parameters lift, lift induced drag, and aerodynamic pitching moment at discrete points along the flight path. At the discrete points, the steady state value of the parameters was calculated. Figure 12, p. 32, shows the steady state equilibrium forces and the relevant angles for the RPV outside and inside the influence of the mothership. The lift of the RPV will be discussed first, followed by the lift induced drag and aerodynamic pitch moment.

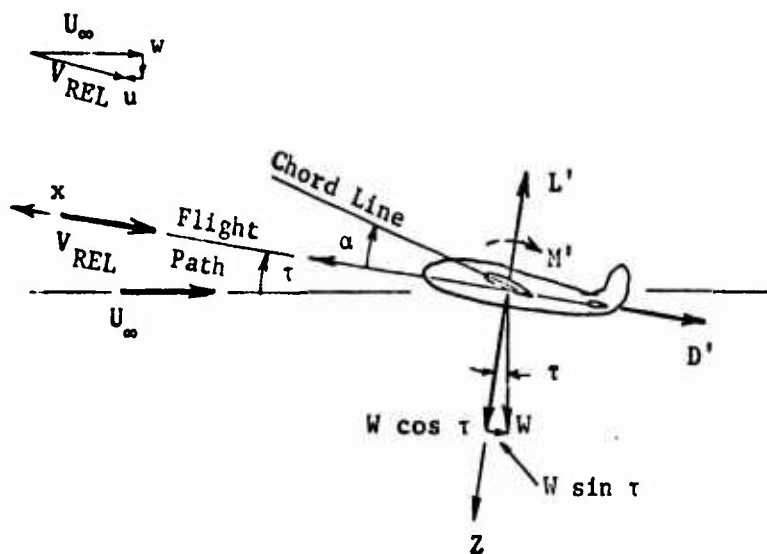
Variation of Lift

The lift of the RPV wing is given by $L = 1/2 \rho V^2 S C_L$. The coefficient of lift C_L is a function of the lift curve slope (a) and the angle of attack (α), i.e., $C_L = a(\alpha - \alpha_{L0})$. For the special case studied a symmetrical airfoil section was assumed so the angle of attack at zero lift (α_{L0}) is zero. The local angle of attack of the RPV wing changes from the free stream angle of attack upon approaching the mothership. Figure 13, p. 33 defines the angles and their relationship. As shown in Fig. 13, the free stream angle of attack (α_∞) of the RPV is decreased by an amount equal to the angle τ inside the influence of the mothership; thus the local angle of attack in the mothership influence is $\alpha = \alpha_\infty - \tau$.

Variation of the local angle of attack across the span and with position relative to the mothership causes a corresponding change in the

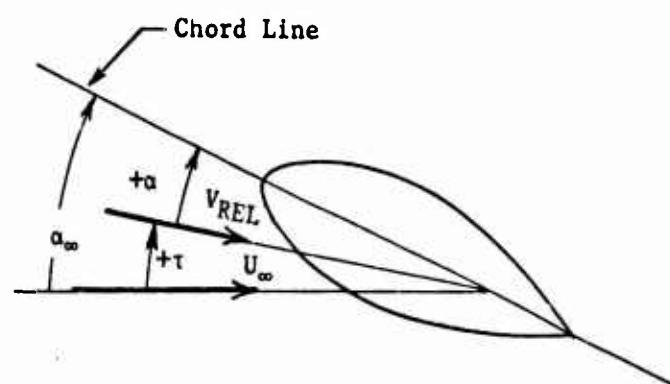


a. Outside Mothership Influence



b. Inside Mothership Influence

Figure 12. Steady Level Flight of RPV



α_∞ = Angle of Attack of the RPV in the Free Stream Outside the Influence of the Mothership.

τ = Angle of the Relative Velocity to the Local Horizontal.

α = Angle of Attack of the RPV with the Relative Velocity Induced by the Mothership. ($\alpha = \alpha_\infty - \tau$)

Figure 13. Definition of Angles

coefficient of lift. Since the lift versus α curve slope ($C_{L_\alpha} = a$) for the RPV is fixed by the airfoil section used, the coefficient of lift varies directly with the change in local angle of attack. The local angle of attack has been assumed constant across the span and equal to the local angle of attack at mid-span so for the wing

$$C_{L_W} = a\alpha = a(\alpha_\infty - \tau) \quad (29)$$

The lift curve slope for the assumed untwisted elliptic RPV wing is computed using

$$a = \frac{\partial C_L}{\partial \alpha} \bigg|_\infty = \frac{a_\infty}{1 + \frac{a_\infty}{\pi AR}} \quad (30)$$

where a_∞ is the theoretical lift curve slope and AR is the aspect ratio (Ref 6:369). The value of a_∞ is 2π (Ref 6:292).

When the RPV is outside the influence of the mothership flying in steady level flight with $L = W$ the lift is computed from

$$L_W = 1/2 \rho_0 U_\infty^2 S C_{L_W} = 1/2 \rho_0 U_\infty^2 S a \alpha_\infty \quad (31)$$

Once the RPV enters the influence of the mothership the lift is computed from

$$L_W = 1/2 \rho_0 V_{REL}^2 S C_{L_W} = 1/2 \rho_0 V_{REL}^2 S a (\alpha_\infty - \tau) \quad (32)$$

The above equation shows that the lift in the influence of the mothership is directly dependent on the relative velocity vector magnitude and direction. To show the variation of the local angle of attack caused by both the change in the relative velocity and the direction of the relative velocity, α was computed from

$$\alpha = \frac{W \cos \tau}{1/2 \rho_0 S a V_{REL}^2} \quad (33)$$

The horizontal tail surface also adds to the total lift of the aircraft. The tail contribution to aircraft lift is

$$L_t \cos \epsilon - D_t \sin \epsilon \quad (34)$$

where ϵ is the downwash angle from the RPV wing. The lift of the tail is computed from

$$L = 1/2 \rho_0 V_{REL}^2 S_t C_{L_t} \quad (35)$$

where S_t is tail area, V_{REL} is the relative velocity of the wing. The tail coefficient of lift is computed for a symmetric airfoil from

$$C_{L_t} = a_t \alpha_t \quad (36)$$

where $a_t = \partial C_{L_t} / \partial \alpha_t$ and α_t is the tail angle of attack. The slope of the tail lift coefficient verse α_t curve (a_t) includes the variation of velocity between the tail (V') and the wing (V_{REL}). The tail angle of attack is

$$\alpha_t = \alpha + i_t - \epsilon \quad (37)$$

and will be negative to produce negative lift for the tail. Thus the lift of the tail is given by

$$L = 1/2 \rho_0 V_{REL}^2 S_t a_t (\alpha + i_t - \epsilon) \quad (38)$$

where i_t is the tail incident angle. The drag of the tail is computed as shown in the following section.

The total lift of the RPV is the sum of the wing generated lift and the components of the tail forces perpendicular to the velocity vector. The total lift was computed by the formula

$$L_{Total} = L_W + L_t \cos \epsilon - D_t \sin \epsilon \quad (39)$$

Variation of Drag

Drag on the RPV wing is given by $D = 1/2 \rho_0 V_{REL}^2 S C_D$. The coefficient of drag for the wing is given by

$$C_D = C_{D0} + k C_L^2 \quad (40)$$

C_{D0} is the coefficient of drag at zero lift and k is a factor to correct for aspect ratio, thickness effects, pressure drag; all drag which varies with angle of attack or lift. The value of k is computed from

$$k = \frac{1}{\pi e AR} \quad (41)$$

where e is the Oswald airplane efficiency factor and AR is the aspect ratio of the wing (Ref 10:7-12).

For a constant C_{D0} and k , the coefficient of drag varies as the square of the lift coefficient. Upon substituting for C_L the coefficient of drag becomes

$$C_D = C_{D0} + k a^2 \alpha^2 \quad (42)$$

Since C_{D0} , k , and a are constant for the RPV the coefficient of drag varies directly with the square of the local angle of attack (α^2) and the square of the relative velocity in the mothership influence. The drag of the wing was computed using

$$D_W = 1/2 \rho_0 V_{REL}^2 S (C_{D0} + \frac{1}{\pi e AR} a^2 \alpha^2) \quad (43)$$

The drag of the tail is computed from

$$D_t = 1/2 \rho_0 V_{REL}^2 S_t C_{Dt} \quad (44)$$

where

$$C_{Dt} = C_{D0t} + k_t C_{Lt}^2 \quad (45)$$

The value of k_t is computed as for the wing.

The total drag of the RPV is the sum of the wing generated drag and the components of the tail forces parallel to the velocity vector. The drag of the fuselage is not included in the model. The total drag was computed by the formula

$$D_{TOTAL} = D_W - L_t \sin \epsilon + D_t \cos \epsilon \quad (46)$$

Variation of Pitch Stiffness

For an aircraft to be statically pitch stable in steady flight the slope of the pitch moment coefficient versus angle of attack curve must be negative ($C_{m_\alpha} < 0$). To determine C_{m_α} the pitching moments acting on the aircraft are determined. Figure 14, p. 38, schematically shows the parameters used in developing the pitch moment equation. The following development uses the notation found in Chapter 6 of Ref 11.

The moments are taken about the aircraft c.g. A positive pitch moment is directed parallel to the positive y-axis and causes a nose up pitch angle. The body contribution to the pitch moment is neglected in this analysis. The wing contribution to the pitch moment is

$$M_w = M_{ac_w} + (L_w \cos \alpha + D_w \sin \alpha)(h - h_{n_w})\bar{c} + (L_w \sin \alpha - D_w \cos \alpha)z \quad (48)$$

The tail contribution to the pitch moment is

$$M_t = M_{ac_t} - l_t [L_t \cos(\alpha - \epsilon) + D_t \sin(\alpha - \epsilon)] - z_t [D_t \cos(\alpha - \epsilon) - L_t \sin(\alpha - \epsilon)] \quad (49)$$

The moment arm l_t for the tail is variable because the c.g. location

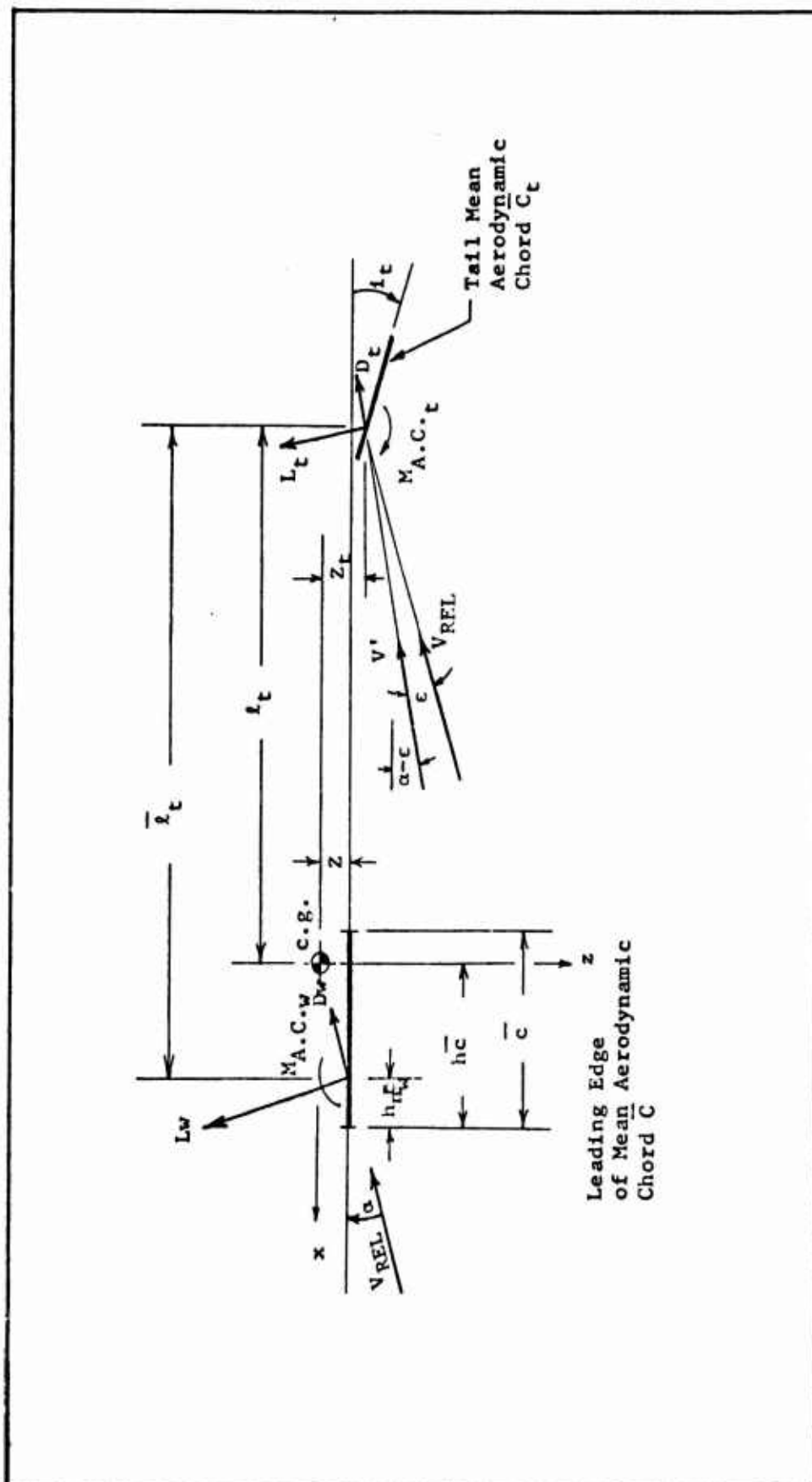


Figure 14. Definition of Pitch Moment Parameters

moves. The mean aerodynamic center location is fixed for fixed wing aircraft so the moment arm l_t can be written in terms of \bar{l}_t and h as

$$l_t = \bar{l}_t - (h - h_{n_w})\bar{c} \quad (50)$$

The total pitching moment, neglecting body contributions, is

$$M = M_w + M_t \quad (51)$$

Thus,

$$\begin{aligned} M = & M_{ac_w} + M_{ac_t} + [L_w \cos \alpha + D_w \sin \alpha](h - h_{n_w})\bar{c} \\ & + [L_w \sin \alpha - D_w \cos \alpha]z \\ & - [L_t \cos(\alpha - \epsilon) + D_t \sin(\alpha - \epsilon)]\bar{l}_t - (h - h_{n_w})\bar{c} \\ & - [D_t \cos(\alpha - \epsilon) - L_t \sin(\alpha - \epsilon)]z_t \end{aligned} \quad (52)$$

The pitching moment coefficient (C_m) is obtained from

$$C_m = \frac{M}{1/2 \rho U_\infty^2 S \bar{c}} \quad (53)$$

To obtain the slope of the pitching moment (M) versus α curve (C_{M_α}) the pitch moment equation is differentiated with respect to α . The result is

$$\begin{aligned} \frac{\partial M}{\partial \alpha} = & \frac{\partial M_{ac_w}}{\partial \alpha} + \frac{\partial M_{ac_t}}{\partial \alpha} \\ & + \left[\frac{\partial L_w}{\partial \alpha} \cos \alpha - L_w \sin \alpha + \frac{\partial D_w}{\partial \alpha} \sin \alpha + D_w \cos \alpha \right] (h - h_{n_w})\bar{c} \\ & + \left[\frac{\partial L_w}{\partial \alpha} \sin \alpha + L_w \cos \alpha - \frac{\partial D_w}{\partial \alpha} \cos \alpha + D_w \sin \alpha \right] z \end{aligned} \quad (54)$$

$$\begin{aligned}
& - \left[\frac{\partial L_t}{\partial \alpha} \cos(\alpha - \epsilon) - L \sin(\alpha - \epsilon) \left(1 - \frac{\partial \epsilon}{\partial \alpha}\right) + \frac{\partial D_t}{\partial \alpha} \sin(\alpha - \epsilon) \right. \\
& \left. + D_r \cos(\alpha - \epsilon) \left(1 - \frac{\partial \epsilon}{\partial \alpha}\right) \right] (\bar{l}_t - (h - h_{n_w}) \bar{c}) \\
& - \left[\frac{\partial D_t}{\partial \alpha} \cos(\alpha - \epsilon) - D_t \sin(\alpha - \epsilon) \left(1 - \frac{\partial \epsilon}{\partial \alpha}\right) \right. \\
& \left. - \frac{\partial L_t}{\partial \alpha} \sin(\alpha - \epsilon) - L_t \cos(\alpha - \epsilon) \left(1 - \frac{\partial \epsilon}{\partial \alpha}\right) \right] z_t
\end{aligned}$$

The partial derivatives $\frac{\partial L_w}{\partial \alpha}$, $\frac{\partial D_w}{\partial \alpha}$, $\frac{\partial L_t}{\partial \alpha}$, and $\frac{\partial D_t}{\partial \alpha}$ are evaluated as follows:

$$\begin{aligned}
a. \quad L_w &= \frac{1}{2} \rho U_\infty^2 S C_L = \frac{1}{2} \rho U_\infty^2 S a \alpha \\
\frac{\partial L_w}{\partial \alpha} &= \frac{1}{2} \rho U_\infty^2 S a
\end{aligned} \tag{55}$$

$$\begin{aligned}
b. \quad D_w &= \frac{1}{2} \rho U_\infty^2 S C_D = \frac{1}{2} \rho U_\infty^2 S (C_{D0} + k(a\alpha)^2) \\
\frac{\partial D_w}{\partial \alpha} &= \rho U_\infty^2 k a^2 \alpha
\end{aligned} \tag{56}$$

$$\begin{aligned}
c. \quad L_t &= \frac{1}{2} \rho U_\infty^2 S_t C_{L_t} = \frac{1}{2} \rho U_\infty^2 S_t a_t (\alpha + i_t - \epsilon) \\
\frac{\partial L_t}{\partial \alpha} &= \frac{1}{2} \rho U_\infty^2 S_t a_t \left(1 - \frac{\partial \epsilon}{\partial \alpha}\right)
\end{aligned} \tag{57}$$

$$\begin{aligned}
d. \quad D_t &= \frac{1}{2} \rho U_\infty^2 S_t C_{D_t} = \frac{1}{2} \rho U_\infty^2 S_t (C_{D0_t} + k_t (a_t \alpha_t)^2) \\
\frac{\partial D_t}{\partial \alpha} &= \rho U_\infty^2 S_t k_t A_t^2 (\alpha + i_t - \epsilon) \left(1 - \frac{\partial \epsilon}{\partial \alpha}\right)
\end{aligned} \tag{58}$$

The total equation for the partial derivative of the aerodynamic pitch moment will not be written out because of its length. The value of C_{m_α} is obtained from

$$C_{m\alpha} = \frac{1}{1/2 \rho U_\infty^2 S \bar{c}} \frac{\partial M}{\partial \alpha} \quad (59)$$

and equations 54, 55, 56, 57, and 58.

In the computation of the aerodynamic pitch moment (C_M) and pitch moment verse α curve ($C_{M\alpha}$) the free stream angle of attack and velocity were used to obtain the free stream values. To obtain the values of C_M and $C_{M\alpha}$ in the influence of the mothership the local angle of attack and relative velocity were used. A symmetrical airfoil section was assumed for both the wing and tail. The non uniform flow field created by the mothership has the effect of a cambering the symmetrical airfoil. The camber created by the non uniform flow field is inversely proportional to the radius of curvature of the flow field. The change in flow field direction was small which implied a large radius of curvature. For this model the camber effect was assumed to be negligible so both the moment about the aerodynamic center and the partial derivative of moment with respect to α were assumed to be zero.

Analysis of Hypothetical RPV

To study the change in aerodynamic forces on the RPV as it approached the docking point, a hypothetical RPV was assumed. The number of vehicle parameters specified for the analysis was kept to a minimum and equations were used in the calculation of the additional parameters. The parameters defining the RPV used in this analysis are given in Table 1, p. 42. The values that were specified are set apart from the calculated values. The parameters given in Table 1 were assumed without performing a preliminary design of the RPV.

A computer program was written to calculate the aerodynamic forces on the RPV. The free stream equilibrium values of the aerodynamic forces

Table 1A. MOTHERSHIPInput

$\alpha_m = 5^\circ$

Aspect Ratio = 10.6

Wing Span = 132.6 ft

Weight = 108,000 lb.

$U_\infty = 300$ knots

Calculated

$\Gamma_o = 861.0809 \text{ ft}^2/\text{sec}$

B. RPVInput

Wing Span = 20.0 ft

Root Chord, Wing = 4.0 ft

$C_{DO_w} = 0.008$

$e_w = 0.8$

$C_{M_o} = 0.0$

Root Chord, Tail = 2.5 ft

$C_{DO_t} = 0.008$

$e_t = 0.8$

$i_t = 4.078^\circ$

$\bar{V}_H = 3.5$

$\bar{l}_t/\bar{c} = 3.5$

$Z = 0.5$ (Low Wing)

$Z_t = 0.25$

$h = 0.15$

$h_{nw} = 0.25$

$h_{nWB} = 0.40$

Weight = 6000 lb.

Initial Closing Velocity = 5 knots

Calculated

Wing Aspect Ratio = 6.4

Wing Area = 62.8 ft²

Wing M.A. Chord = 3.4 ft

Wing $C_{L_\alpha} = a = 0.0835/\text{deg}$

Tail Aspect Ratio = 4.2

Tail Span = 8.2 ft

Tail Area = 16.2 ft²

Tail M.A. Chord = 2.12 ft

Tail $C_{L_\alpha} = a_t = 0.0743/\text{deg}$

$\bar{l}_t = 11.88$ ft

$\Gamma_o = 332.76 \text{ ft}^2/\text{sec}$

$\alpha_m = 3.87^\circ$

$C_L = 0.324$

$C_D = 0.0146$

$C_{M_\alpha} = -0.320$

were calculated. Then the equilibrium values for the aerodynamic forces were calculated inside the mothership influence. To show the variation in values along the assumed flight path, the point of analysis was moved in discrete steps until the docking point was reached. The last point on each of the plots in Figures 15 through 24 correspond to the docking point.

In the analysis the RPV was moved from a point approximately 1.3 mothership wing spans to the rear and level with the docking point. The gradual increase in altitude indicated in the description of the flight path corresponds to a distance equal to approximately 0.38 wing spans. If the RPV had been allowed to make the gradual increase in altitude at a climb angle equal to the deflection of the velocity vector, a distance equal to approximately 43 wing spans would have been required. The decrease in RPV velocity as it approaches the docking point is shown in Figure 15, p. 44. The flight tests of the XF-85 showed a decrease in velocity as the docking point was approached. Figures 16, 17, and 18, p. 45, 46, and 47, show the change in lift, C_L , and angle of attack respectively. The increase in angle of attack comes primarily from the decrease in velocity which requires that the angle of attack be increased to maintain the necessary lift. The increase in C_L is a direct result of the increase in angle of attack. The increase in lift is the combined result of the decreased velocity and increased angle of attack.

The variation of C_D , lift induced drag, and thrust are shown in Figures 19, 20, and 21, p. 48-50. The value of C_D is increased as the docking point is approached due to the increase in angle of attack. The lift induced drag increases as the docking point is approached. The increase in thrust is just equal to the increase in drag in steady flight.

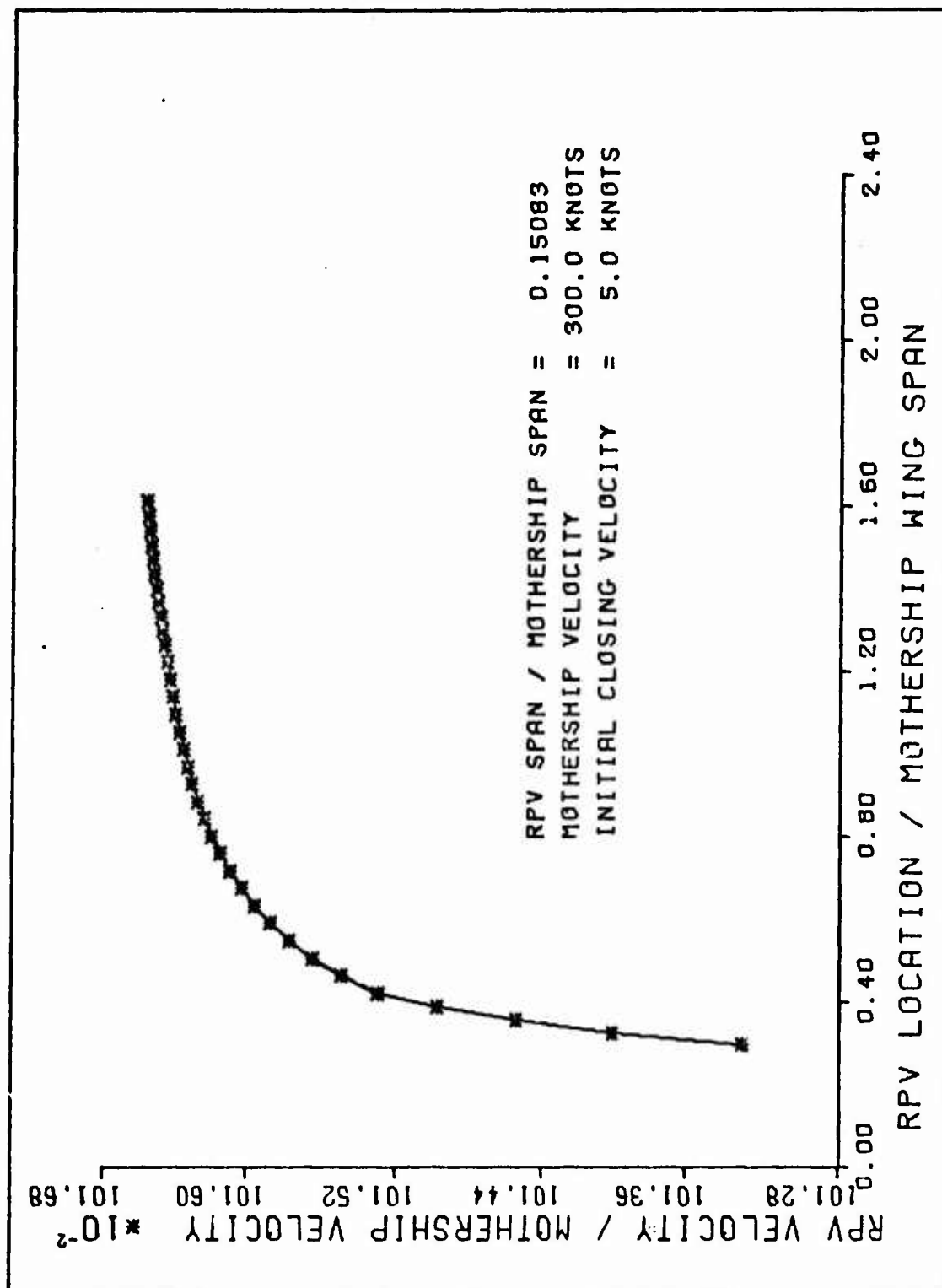


Figure 15. Velocity Change of RPV

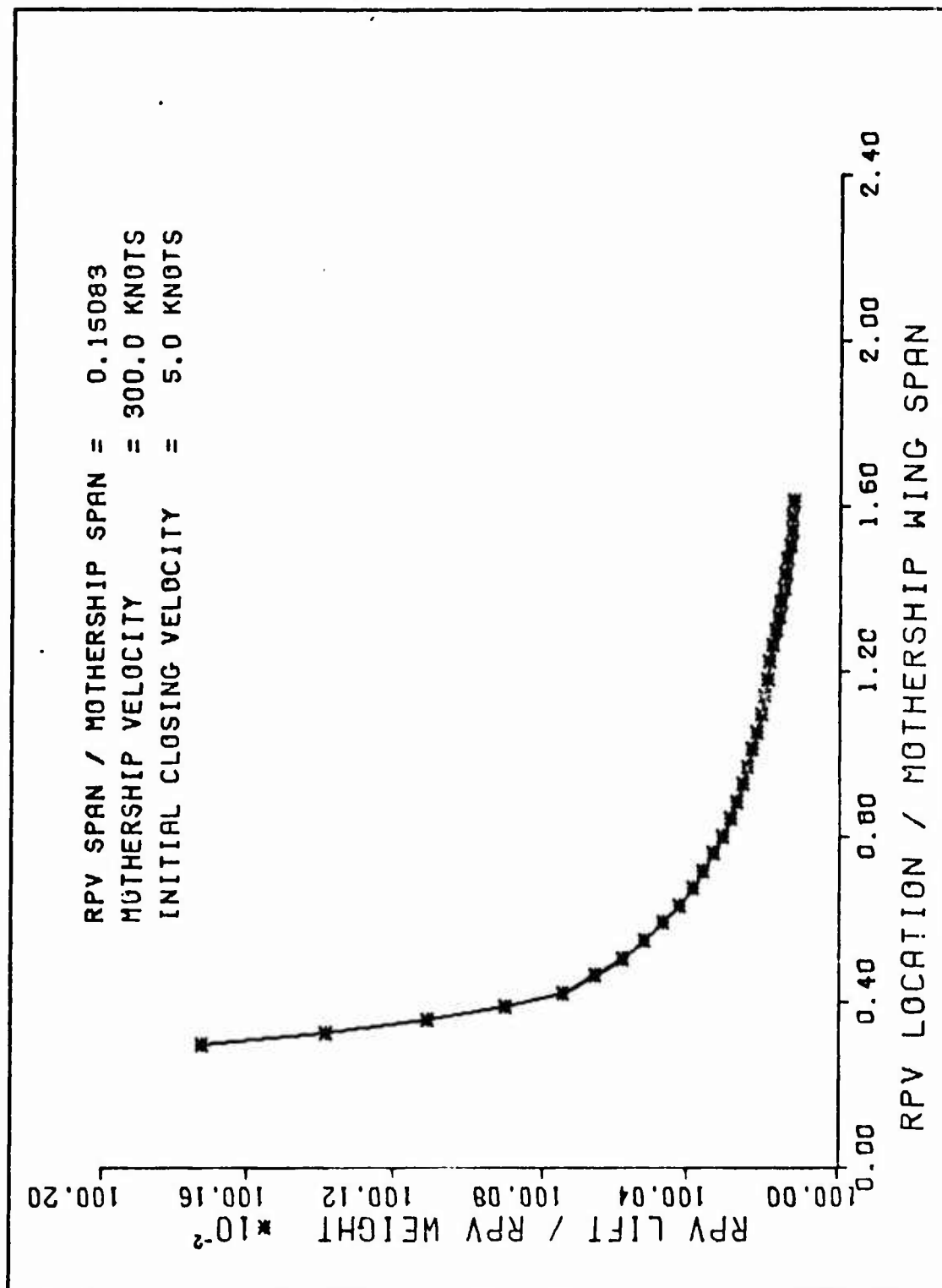


Figure 16. Lift Change of RPV

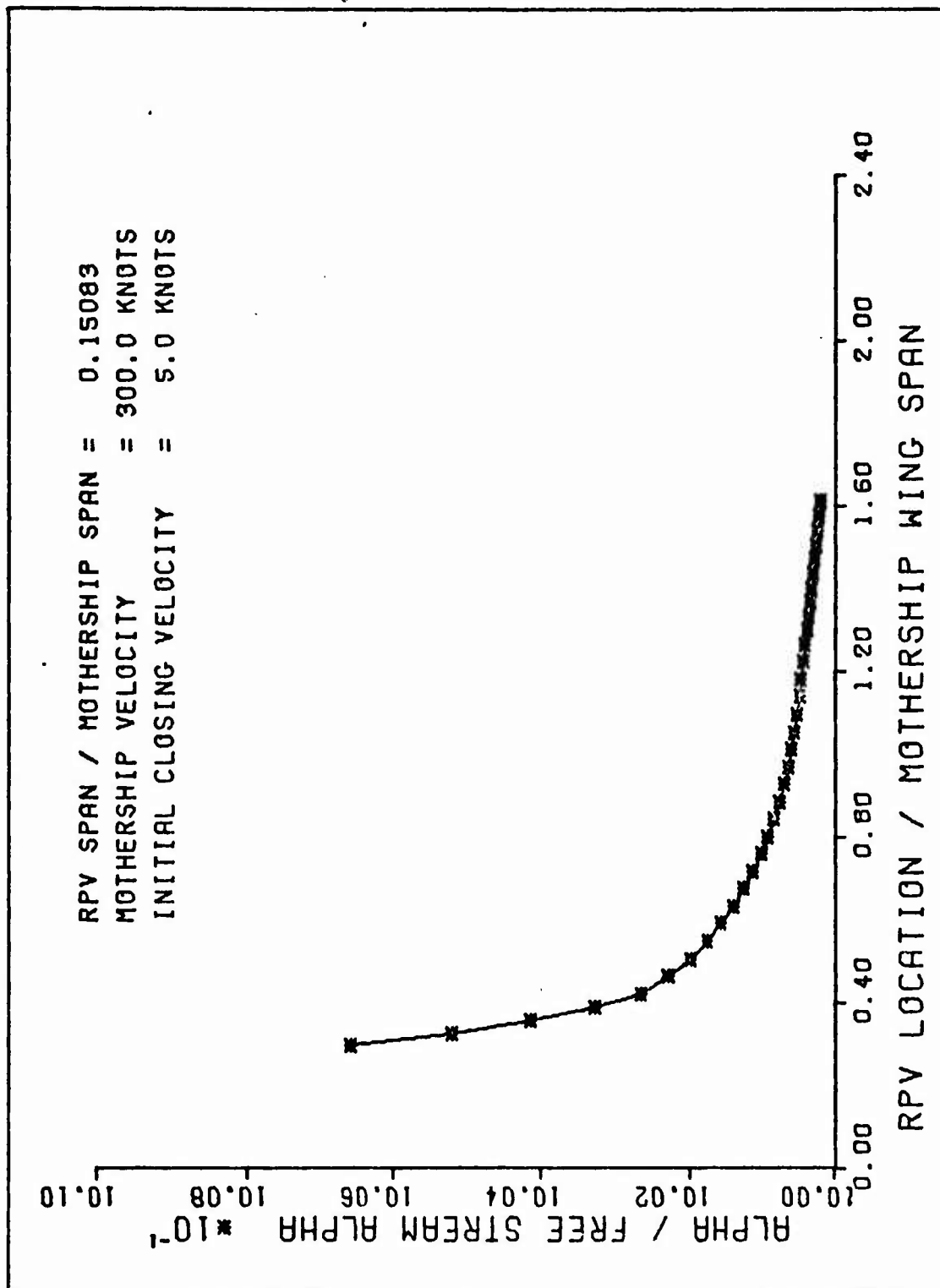


Figure 18. Angle of Attack Change

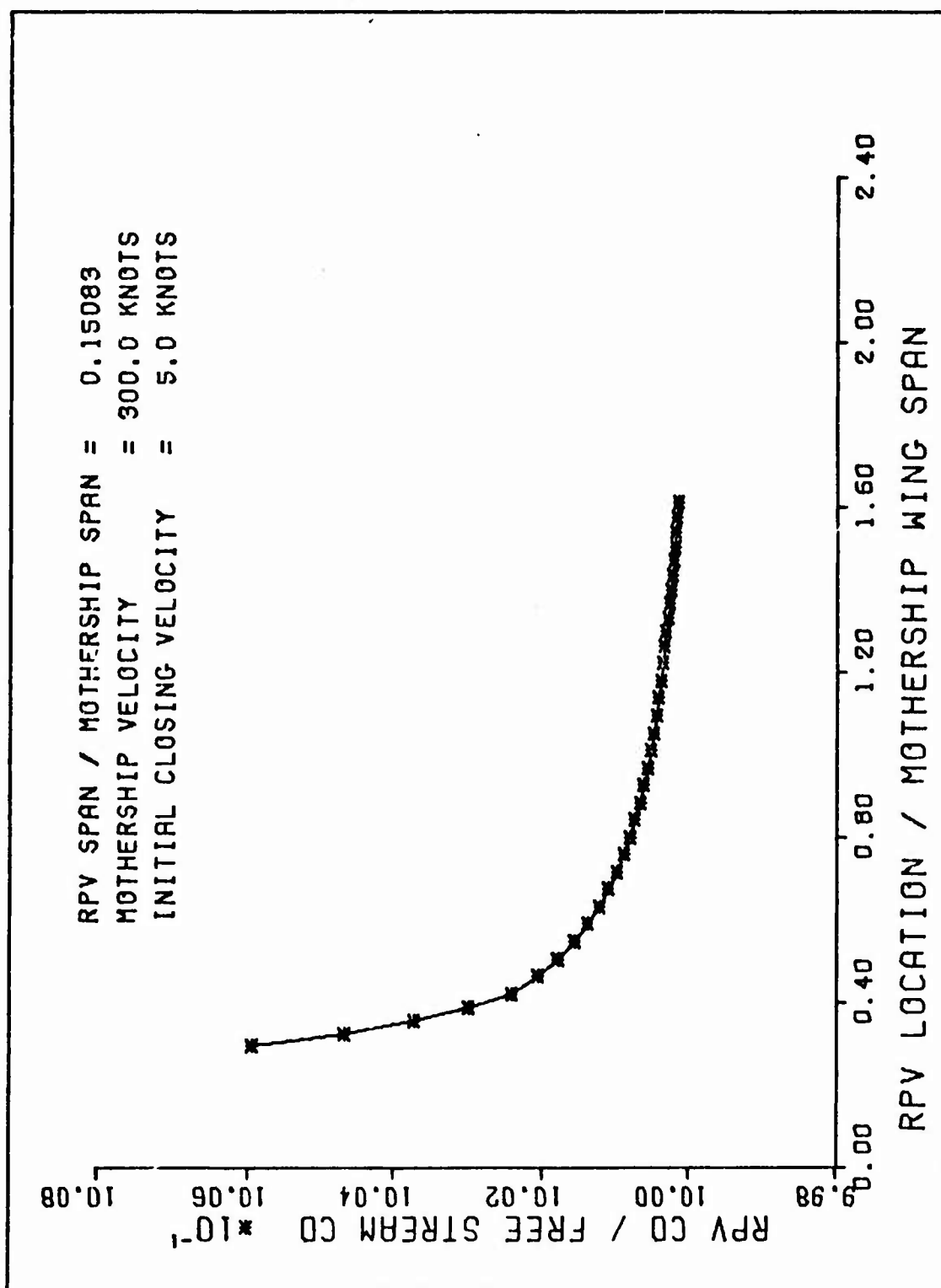


Figure 19. Change in Coefficient of Drag

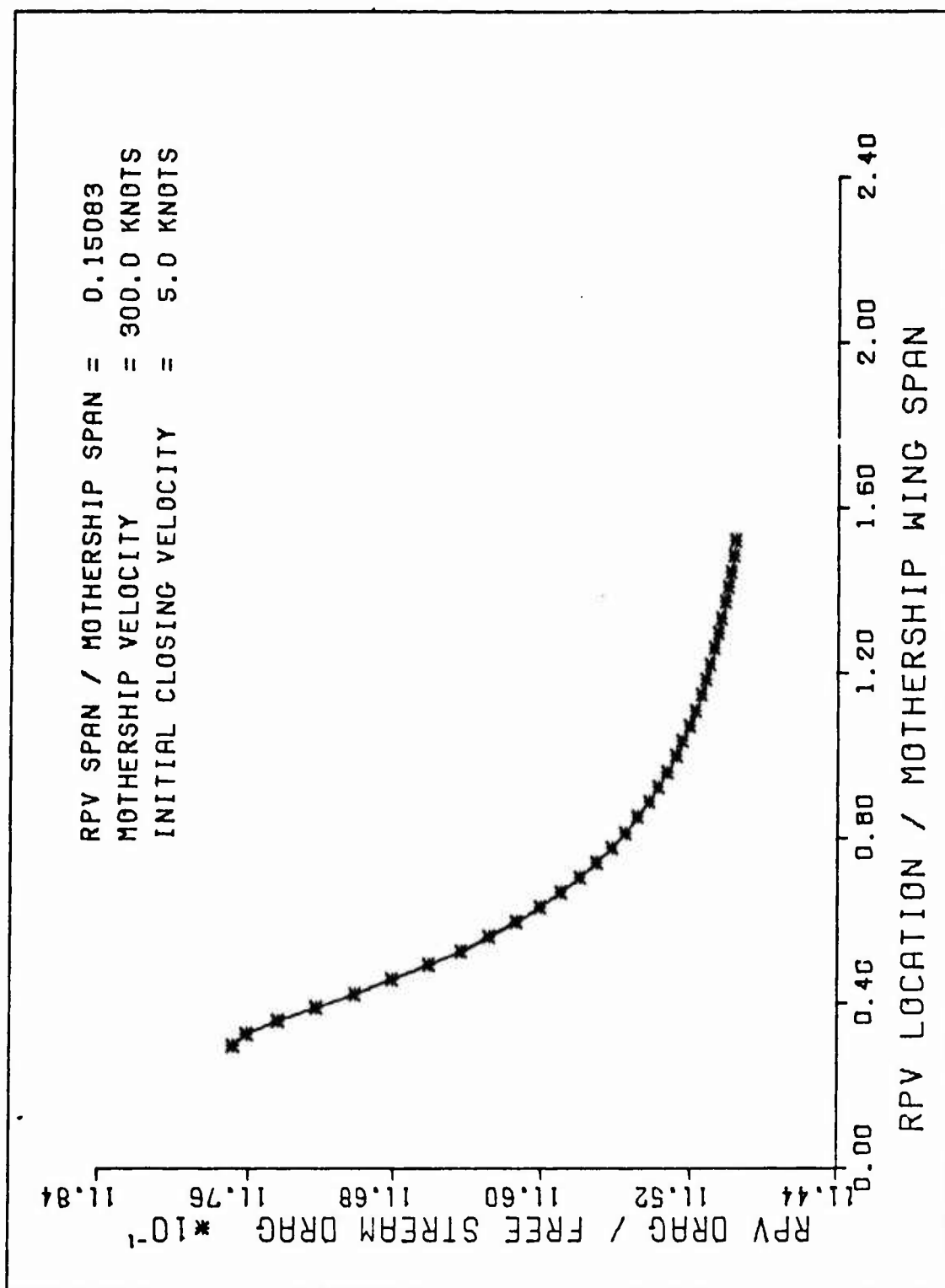


Figure 20. Drag Change of RPV

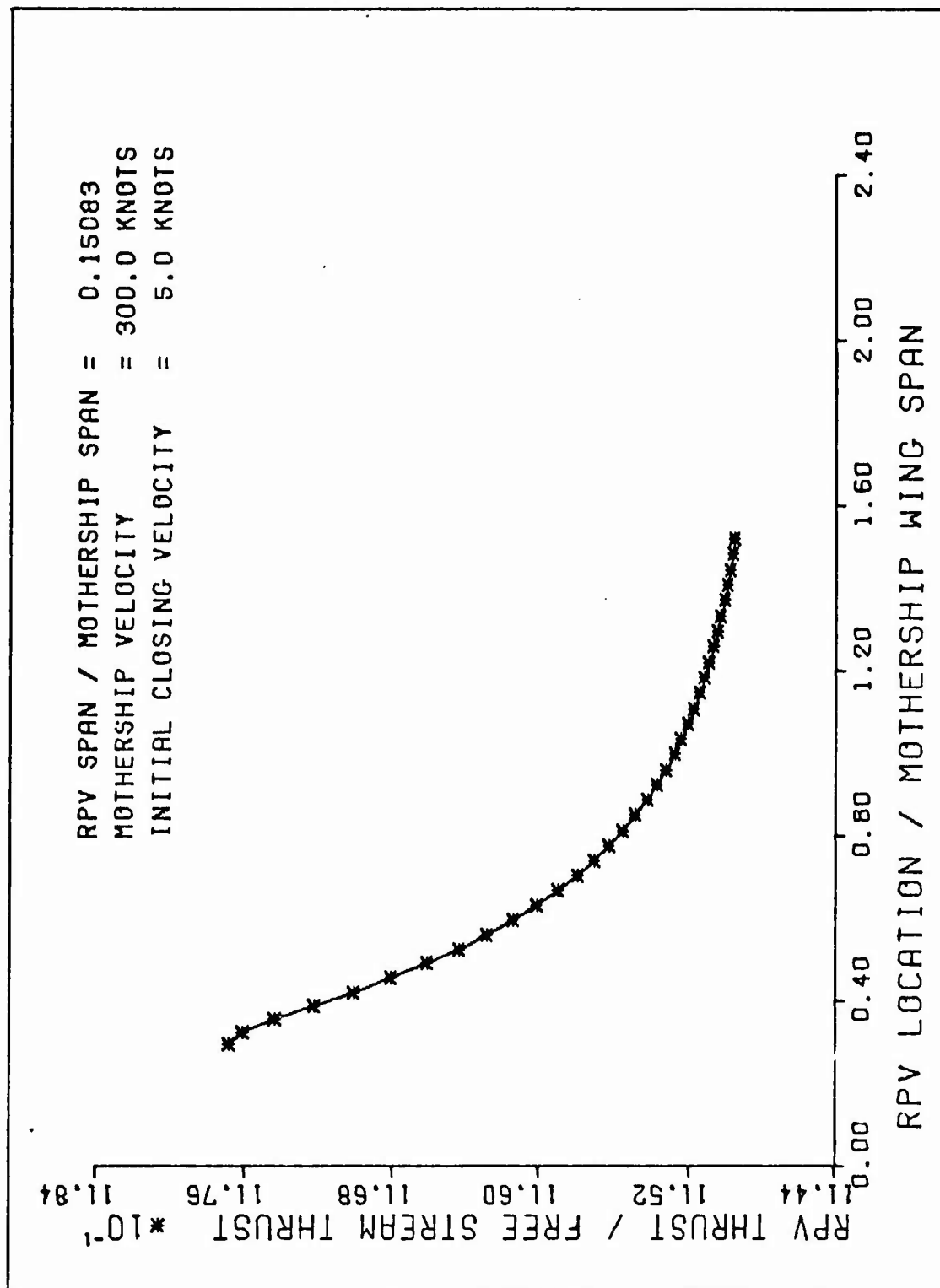


Figure 21. Thrust Change of RPV

The XF-85 flight tests showed a drastic increase in drag and thus thrust as the docking point was approached.

The variation in static pitch stability (C_{M_α}) is shown in Figure 22, p. 52. As the docking point is approached the slope of the C_M versus α curve decreases in negative value which corresponds to a decrease in aerodynamic pitch stability. The flight tests of the XF-85 indicated that the vehicle became marginally stable as the docking point was approached due to the excessive control manipulations required to maintain a steady position for the final hook-on.

The decrease in the closing velocity is shown in Figure 23, p. 53. The closing velocity is the difference of the x-component of the RPV velocity and the mothership velocity. The time required to reach the docking point is shown in Figure 24, p. 54. The time plot indicates the time span covered in the analysis.

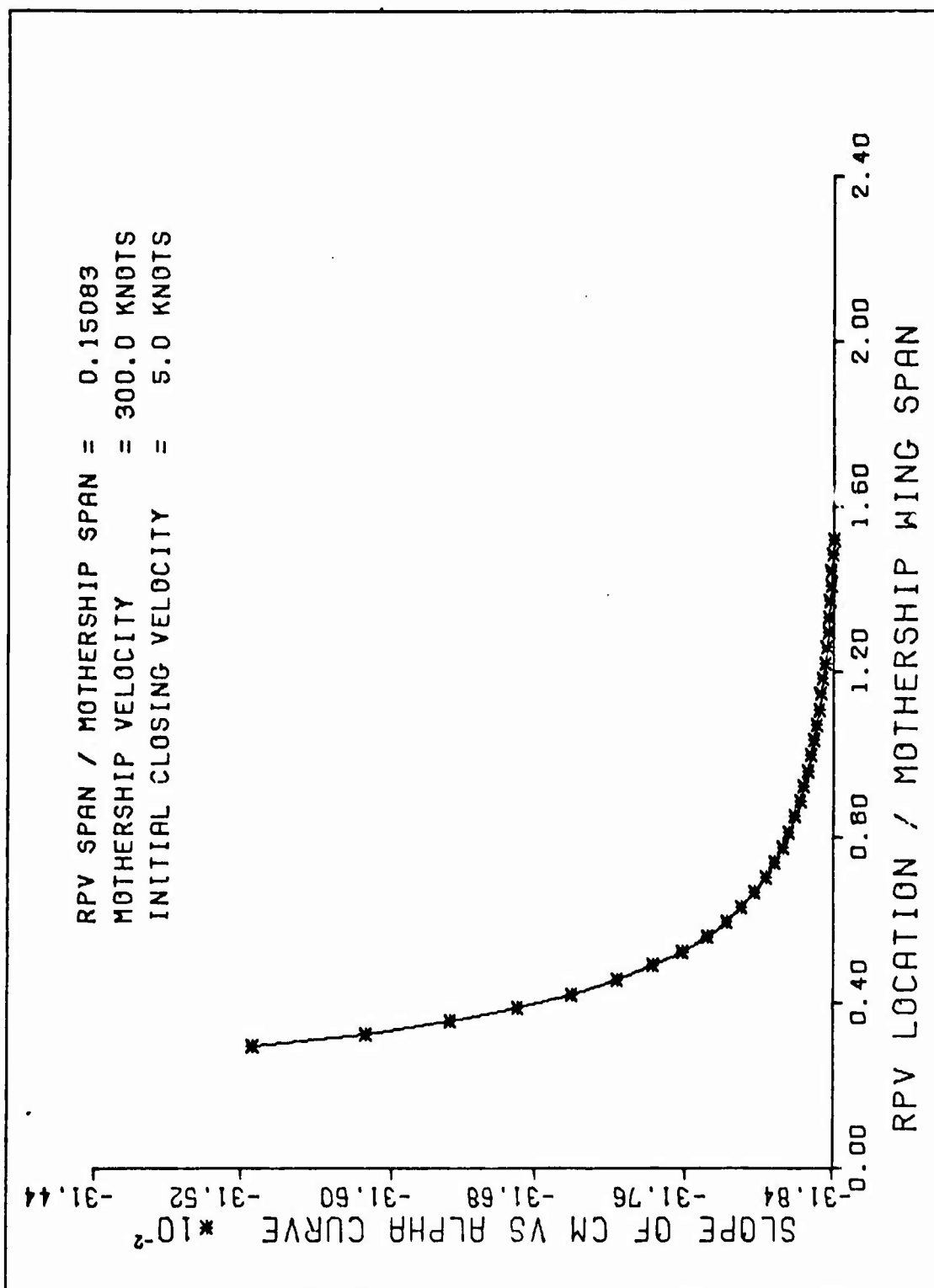


Figure 22. Change in RPV Static Pitch Stability

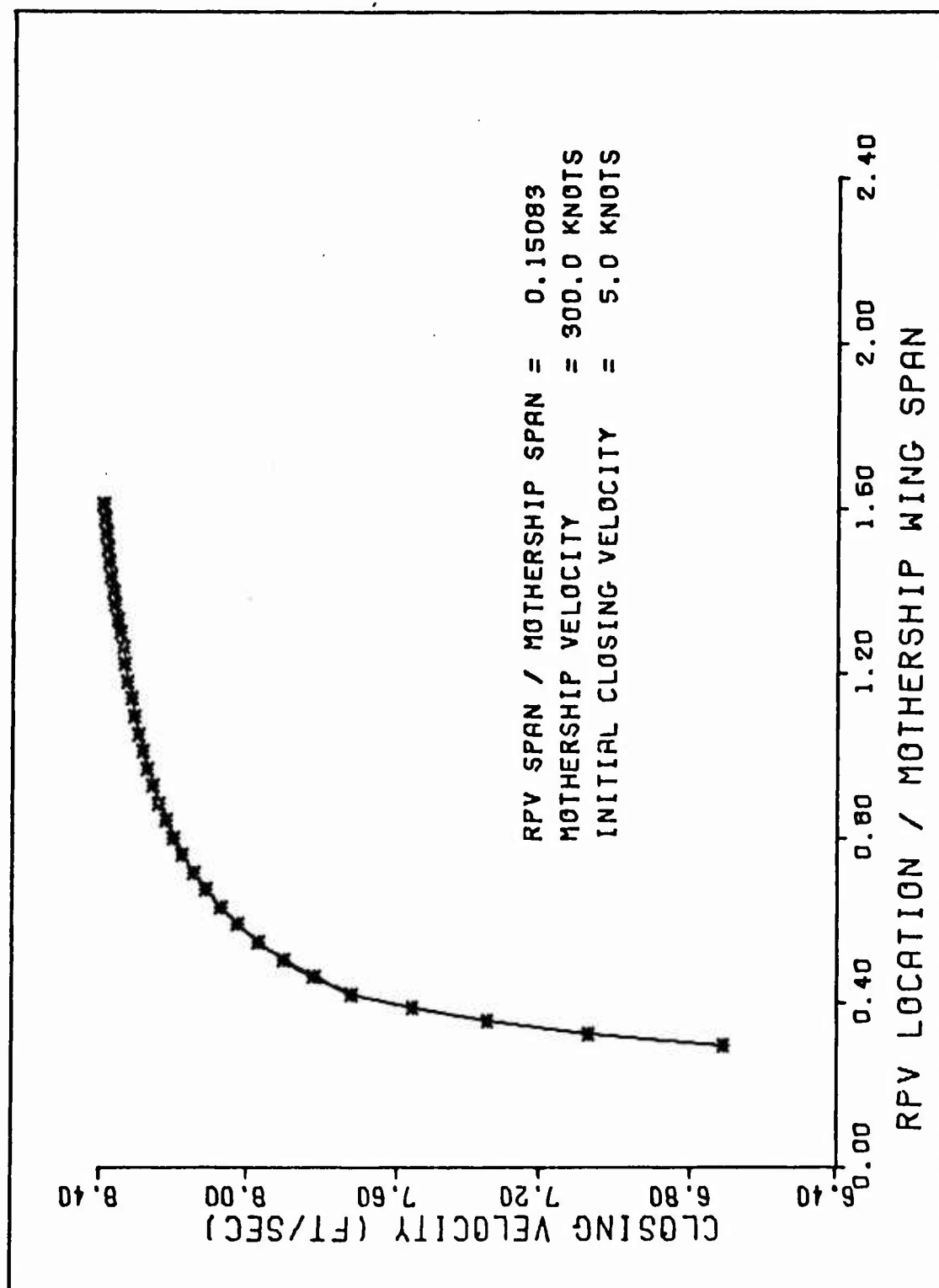


Figure 23. Closing Velocity

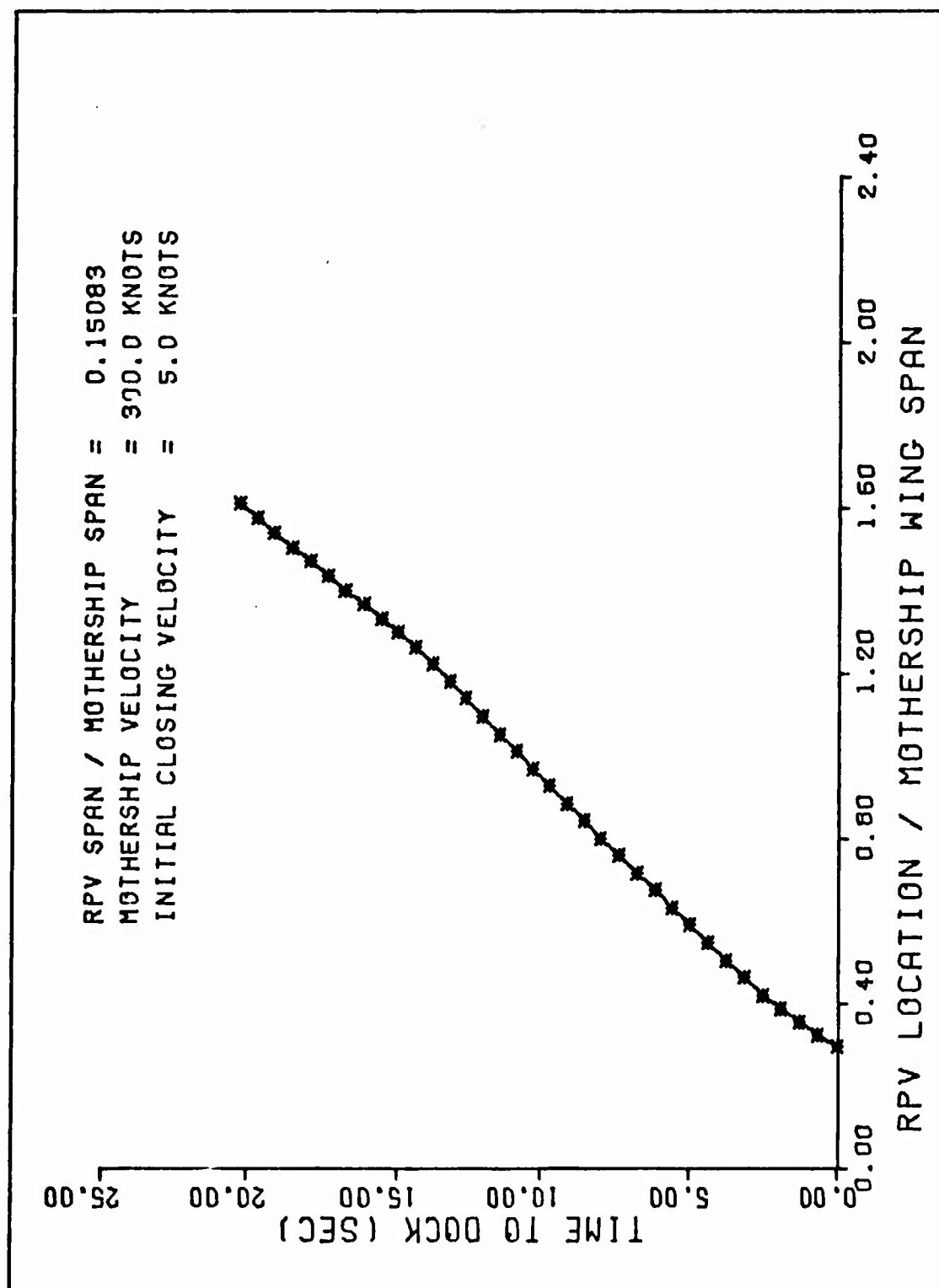


Figure 24. Time to Dock

V. Conclusions and Recommendations

Conclusions

A steady state aerodynamic analysis was performed on the integrated launch/recovery system proposed for in-flight capture of a RPV. The analysis was performed by modeling the mothership, wing only, with a bound vortex having an elliptic distribution of circulation across the span and two trailing vortices of constant circulation. The mothership flow field, which was the induced velocity generated by the mothership model, was used to calculate the steady level flight aerodynamic forces of lift, lift induced drag, and pitch moment.

The comparison of results obtained from the analysis, with the XF-85 flight tests showed that the trend of the change in aerodynamic forces was correctly predicted for the lift, drag, and pitch moment. The aerodynamic analysis was performed on a hypothetical RPV. The analysis may be applied to an actual RPV/mothership system to obtain an initial understanding of the variation in aerodynamic forces as the RPV approaches the mothership.

Recommendations

The purpose of modeling the mothership was to investigate the mothership effects on the RPV as it approached the docking point. By modeling the mothership as a horseshoe vortex representing the wing, the only effect studied was that of the wing. An improvement in the model of the mothership may be made by representing the body with a distribution of point sources along the axis of the fuselage and the tail with a horseshoe vortex. In formulating the horseshoe vortex model it was assumed that the RPV would be farther than two chord lengths away from the center of pressure of the

wing. This may not be the case for some potential mothership capture systems. Thus if the trapeze docking head is located closer than two chord lengths from the center of pressure, the wing probably should be modeled as a vortex sheet. The horseshoe vortex model of the mothership may be used to generate a unsymmetrical velocity field relative to the mothership by moving the point of analysis off the plane of symmetry. The unsymmetrical flow field generated may then be used in analyzing the dynamic stability of the RPV as it approached the mothership.

Cited References

1. Jones, R.T. "New Design Goals and a New Shape for the SST." Astronautics and Aeronautics, 10:66-70 (December 1972).
2. Barkey, H.D. XF-85 Parasite Fighter Design and Development Summary. Report No. 1226, 1 September 1949, McDonnell Aircraft Corp., St. Louis.
3. Anderson, C.E. "Pilot Comments and Summary of a Qualitative Evaluation of a Prototype Parasite Fighter Launching and Retrieving Trapeze Mechanism Installed on a B-57 and F-84E Combination." Technical Note WCT-52-62, Wright-Patterson AFB, Ohio (December 1952).
4. Glauert, Hermann. The Elements of Aerofoil and Airscrew Theory. New York: The MacMillan Company, 1944.
5. Milne-Thomson, L.M. Theoretical Aerodynamics. New York: MacMillan and Company, LTD., 1958.
6. Houghton, E.L. and Brook, A.E. Aerodynamics for Engineering Students, London: Edward Arnold LTD., 1970.
7. Karamcheti, Krishnamurty. Principles of Ideal-Fluid Aerodynamics. New York: John Wiley & Sons, Inc., 1966.
8. Hodgman, Charles D., Editor. Standard Mathematical Tables (12th Edition). Cleveland: Chemical Rubber Publishing Company, 1963.
9. McEwan, J. XF-85 Parasite Fighter Phase I Flight Test Report. Report No. 1181, 24 May 1949, McDonnell Aircraft Corp., St. Louis.
10. Corning, Gerald. Supersonic and Subsonic Airplane Design. Ann Arbor: Edwards Brothers, Inc., 1953.
11. Etkin, Bernard. Dynamics of Atmospheric Flight. New York: John Wiley & Sons, Inc., 1972.

Appendix A

Computer Program

A computer program was written to perform the calculation of steady aerodynamic forces at discrete points relative to the mothership model. Comment cards were used throughout the computer program to indicate what was done in each part of the program. A simplified flow diagram is given in Figure 25. A copy of the computer program begins on page 60.

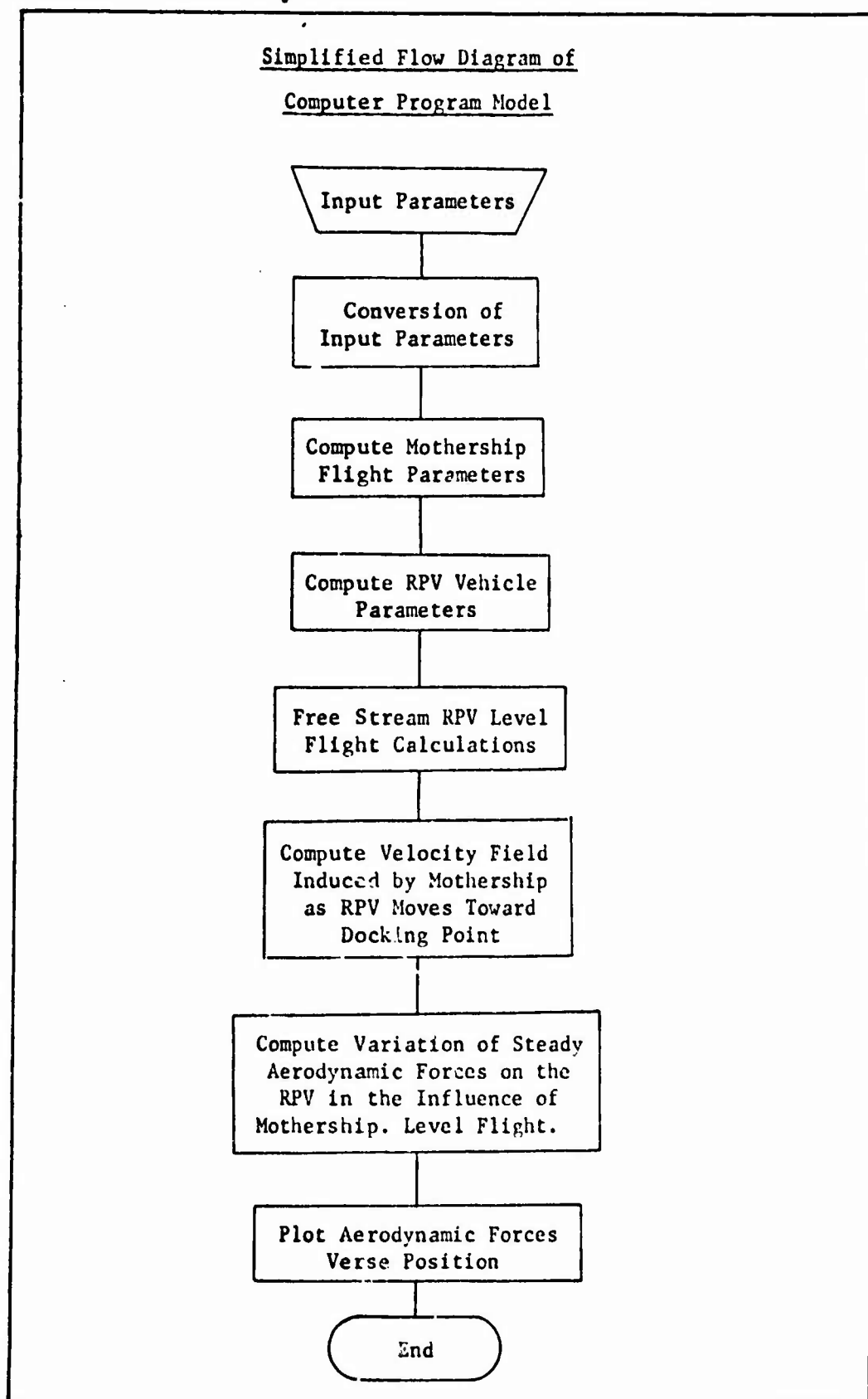


Figure 25. Simplified Flow Diagram

```

C
FRCGPAM RPV (INPUT, OUTPUT, PLCT)

COMMON P1, P2, P3, S
DIMENSION PP(40), FATIOPS(40)
DIMENSION ZLIFT(5), DRAG(5)
DIMENSION VPELP(40), ZLPPVP(40), DRAGF(40)
DIMENSION WP(40), T(40), CMA(40)
DIMENSION ANSI(5), F2I(5)
DIMENSION U(5), V(5), W(5)
DIMENSION VPEL(5), WEL(5)
DIMENSION CH(5), HCD(5)
DIMENSION GANCR(5), KWASHR(5), ERPV(5), ERPV(5)
DIMENSION TAU(5), TAU(5), ALP1(5), ALP1(5)
DIMENSION CL3(5), CF3(5), ZLRPV3(5), CRAG2(5)
DIMENSION CLT3(5), COT3(5), ZLRPV3(5), DRAG13(5)
DIMENSION F2(5), FOWEQ3(5), H03(5)
DIMENSION P(40)
DIMENSION OG4NWA(40)
DIMENSION VPEL(40)
DIMENSION PITCHPL(5), CML(5)
DIMENSION PLWAL(5), PMFAL(5), PLTAL(5), PCIPAL(5)
DIMENSION PWINGL(5), PTAIL(5), PMFAL(5), CHAL(5)
DIMENSION VPPV(5), CLOSVP(5), TIME(5)
DIMENSION WPOVE(40), CLOSVP(40), TIME(40)
C-----COMPUTE THE INDUCED VELOCITY FROM THE WCRSPACE VORTEX FILAMENT MODEL
C      OF MOTHERSHIP WING.
C-----
C
C      AINF = THE THEORETICAL 2-DIMENSIONAL LIFT CURVE SLOPE.
C      ALFAP = THE ANGLE OF ATTACK OF THE MOTHERSHIP WING IN DEGREES.
C      ALFPA = THE ANGLE OF ATTACK OF THE MOTHERSHIP WING IN RADIAN.
C      ANS = THE VALUE OF THE INTEGRAL FOR THE MOTHERSHIP PCUNE
C           VORTEX FILAMENT.
C      ACFAFS = THE ANGLE OF ATTACK OF THE RPV IN THE FREE STREAM VELOCITY.

```

ACFAL = THE ANGLE OF ATTACK OF THE RPV WING WITH THE RELATIVE VELOCITY.
 ACP = THE SLOPE OF THE MOTHERSHIP COEFFICIENT OF LIFT VERSES ANGLE OF
 ATTACK CURVE.
 ARP = THE ASPECT RATIO OF THE MOTHERSHIP WING.
 ARPV = THE LIFT CURVE SLOPE FOR THE RPV.
 ARPV = THE ASPECT RATIO OF THE RPV WING.
 EARLT = THE LENGTH ELIATED FROM THE M.A.C. OF WING
 AND THE M.A.C. OF THE TAIL.
 BLTECH = THE RATIO OF TAIL AND CHORD.
 ERPV = THE SPAN OF THE RPV WING IN FEET.
 CEIAR = THE MEAN AERODYNAMIC CHORD OF THE RPV WING.
 CEIAR = THE INCLUDED WING COEFFICIENT.
 CCC = THE COEFFICIENT OF DRAG OF RPV WING AT ZERO LIFT.
 CMARV = THE FITTING MOMENT COEFFICIENT OF THE RPV ABOUT THE
 RPV CENTER OF GRAVITY.
 CRCCIT = THE FUEL CHORD OF THE RPV TAIL.
 CRCCIT = THE FUEL CHORD OF THE RPV WING.
 CIEPV = THE INCLUDED DRAG OF THE RPV.
 F = THE AIRPLANE EFFICIENCY FACTOR (COUNTING P. 7-12).
 EP = THE CORRECTION ANGLE FROM THE MOTHERSHIP.
 ERPV = THE CORRECTION ANGLE FOR THE RPV.
 CAPCH = THE STRENGTH OF THE CIRCULATION AT THE CENTER OF THE
 MOTHERSHIP ELLIPTICAL WING.
 P = THE LOCATION OF THE RPV C.G. MEASURED FROM THE LEADING EDGE
 OF THE MEAN AERODYNAMIC CHORD AS A PER CENT OF THE MEAN
 AERODYNAMIC CHORD.
 PAMP = THE LOCATION OF THE WING-BODY NEUTRAL POINT, MEASURED FROM THE
 LEADING EDGE OF THE MEAN AERODYNAMIC CHORD, AS A PER CENT OF
 THE MEAN AERODYNAMIC CHORD.
 PE = THE MORSELENS REQUIRED FOR STRAIGHT AND LEVEL FLIGHT.
 A = VARIABLE TO CONTROL PRINTING OF CLIPIT DEPENDENT ON FLIGHT
 CONDITION.
 F = THE LOCATION OF THE RPV WING, WITH COMPONENTS (F1, F2, F3).
 FI = THE TRIGONOMETRIC CONSTANT FI.
 FCMREC = THE FORCE REQUIRED FOR STRAIGHT AND LEVEL FLIGHT.
 RPO = THE DENSITY AT ALTITUDE. FOR AIR AT SEA LEVEL,
 $RPO = 0.002378 \text{ LBF} / (\text{SEC}^2) / (\text{FT}^3)$
 RP = THE AMOUNT THE TRAILING VORTEX IS AWAY FROM THE MOTHERSHIP
 WING TIP. FOR AN ELLIPTICALLY LEADED WING, $RP = F1/4$.
 S = THE SEMI-SPAN OF THE MOTHERSHIP WING IN FEET.



Reproduced from
best available copy.

```

C SRPV = THE SPAN-SPAN OF THE RPV WING IN FEET.
C S1 = THE SPAN OF THE MOTHERSHIP WING IN FEET.
C LINF = THE FREE STREAM VELOCITY IN KNOTS CONVERTED TO FEET PER SECOND
C BY KNOTS*1.68494 = FEET PER SECOND (EQUIVALENT AIR SPEED).
C VEEL = THE MAGNITUDE OF THE THE RELATIVE VELOCITY OF THE RPV.
C VPEAR = THE HORIZONTAL-TAIL VOLUME RATIO REFERENCED TO THE MEAN
C AERODYNAMIC CENTER OF WING-FOXY COMBINATIONS.
C WAPRV = THE WING AREA OF THE RPV IN SQUARE FEET.
C WAPMV = THE LIFT REQUIRED FROM WING TO BALANCE THE NEGATIVE
C LIFT OF THE TAIL IN FREE STREAM FLIGHT.
C WAPVR = THE WEIGHT OF THE RPV IN POUNDS.
C WPM = THE WEIGHT OF THE MOTHERSHIP IN POUNDS.
C WMPRV = THE LIFTING MOMENT OF THE RPV WING ABOUT THE CC.
C ZLP = THE LIFT OF THE MOTHERSHIP WING IN 2-D STEADY LEVEL
C FLIGHT ZLM = WEIGHT OF THE MOTHERSHIP IN LBF.
C ZLRPV = THE LIFT OF THE RPV.

```

END OF SYMBOL DEFINITIONS

PARAMETERS THAT MUST BE SET IN THE PROGRAM

```

FI = 3.1415926536
ALCFPV = 0.0
ALFPM = 0.0
ALFMDA = ALFPM * (.7174533
ACP = 2.0 * FI
APR = 10.6
ELFLM = 3.5
CFPV = 20.0
CCC = .009
CCCT = 0.008

```

[illegible]

```

S = ( S1 / 2.0 )
C SEPI-SFAN OF TRAILING VORTEX SYSTEM.
SE = S * QM
CAPCM = ( 2.0 * WM ) / ( PI * C * S * APS(LJNF) )
ZLIFTM = (PI/4.0) * C * Q * LINE * GAWCM * S1
CRAGIM = (PI/4.0) * C * Q * (GAWCM * 2.0)
%*****
%***** OUTLET FLOWMATE *****
%*****
PRINT 1725, WING
1025 FORMAT( ' THE FREE STREAM VELOCITY (FT/SEC) IS', F15.7)
PRINT 7500, VM
7500 FORMAT( ' MOTHERSHIP VELOCITY (FT/SEC) IS ', 0X, F15.7)
PRINT 1000, GAWCM
1000 FORMAT( ' GAMMA 0 FOR THE MOTHERSHIP IS = ', 12X,
1 F15.7, ' SOLIDE FEET PER SECOND.' )
PRINT 6000, ZLIFTM
6000 FORMAT( ' THE LIFT OF THE MOTHERSHIP IS ', 0X,
1 F15.7, ' IN POUNDS.' )
PRINT 6001, C * ACIM
6001 FORMAT( ' THE INDUCED DRAG ON THE MOTHERSHIP IS', F20.7,
1 ' IN POUNDS.' )
C ***** END OF MOTHERSHIP CALCULATIONS *****
C *****
C ***** RPV VEHICLE PARAMETER CALCULATIONS *****
C *****
C SEPI-SFAN OF RPV WING.
SEFN = 2 * FN / 2.0
C GEOMETRIC CHORD OF RPV WING.
CECCM = ( FI / 4.0 ) * CROOTM
C GEOMETRIC CHORD OF RPV TAIL.
CECTT = ( PI / 4.0 ) * CPOOTT
C MEAN AERODYNAMIC CHORD OF RPV WING.
CEARF = ( 6.7 * CROOTM ) / ( 3.0 * FI )
C MEAN AERODYNAMIC CHORD OF RPV TAIL.
CEART = ( 6.0 * CPOOTT ) / ( 3.0 * FI )

```



```

C TOTAL PREL STRAP LIFT.
TCLIFT = ZLRPVLF + ZLRPVTLCOS(ERPVLF) - CRAGTLF*SIN(ERPVLF)
C TOTAL PREL STRAP DRAG.
TCLDRAG = DRAGLF - (ZLRPVTLSIN(ERPVLF) + (CRAGTLF*CCS(ERPVLF))
C PREL STREAM THRUST.
T1 = TOLCDRG
C PREL STREAM POWER.
PCHRGCL = T1 * ARS(VRPVF)
C PREL STREAM WAKEFINGER.
WFI = PCHRGCL/SEC
C PREL STREAM PITCHING MOMENT.
PITCHLF = WIPACK + PITMCT
1 * (ZLRPVLF*CCS(ALPINF1) + DRAGLF*SIN(ALPINF1))
2 * (M - WIMU) * CRAG
3 * (ZLRPVLF*SIN(ALPINF1) - DRAGLF*CCS(ALPINF1)) * 7
4 * (ZLRPVTLCOS(ALPINF1) - ERPVLF) + DRAGTLF*SIN(ALPINF1)
5 * (ZLRPVLF)*IFALT - (M - WIMU) * (CRAG)
6 * (CRAGTLF*CCS(ALPINF1) - ERPVLF)
7 * (ZLRPVTLSIN(ALPINF1) - ERPVLF) * 71
C PREL STREAM PITCHING MOMENT COEFFICIENT.
CMLES = PITCHLF / (L*MC/2.0)*(ARS(VRPVF)**2.0)*WARPV*CEARR)
C COMPUTING THE PREL STREAM PARTIAL DERIVATIVES FOR STATIC PITCH MOMENT.
FLPVLF = (FMC/2.0)*WARPV*AROV*(AFS(VRPVF)**2.0)
FDPVLF = WIMU*CA*AROV**2.0)*ALPINF1*(AFS(VRPVF)**2.0)
FLTPVLF = (FMC/2.0)*TAROV*AROV*(1.0 - FEPA)*(ARS(VRPVF)**2.0)
FLTPVLF = WIMU*TAROV*CT*(ARPV**2.0)*(ALPINF1 + ITNCIC - ZRPVLF)
1 * (1.0 - FEPA)
C COMPUTING DERIVATIVE OF PITCH MOMENT WITH RESPECT TO ANGLE OF
ATTACK FOR THE PREL STREAM.
FPIVLF =
1 * (FLPVLF*CCS(ALPINF1) - ZLRPVLF*SIN(ALPINF1)
2 * FDPVLF*SIN(ALPINF1) + DRAGLF*CCS(ALPINF1) )
3 * (M - WIMU) * CRAG
4 * (FLPVLF*SIN(ALPINF1) + ZLRPVLF*CCS(ALPINF1)
5 * FDPVLF*CCS(ALPINF1) + DRAGLF*SIN(ALPINF1)) * 2
FPAVLF =
1 * (FLTPVLF*CCS(ALPINF1) - ZRPVLF *
2 * SIF(ALPINF1 - ERPVLF)*(1.0 - FEPA) + FCTPVLFSIN(ALPINF1
3 * - ERPVLF) + CRAGTLF*CCS(ALPINF1 - ERPVLF)*(1.0 - FEPA) )
4 * (IFALT - (M - WIMU)*CRAG) - (FCTPVLFSIN(ALPINF1 - ERPVLF)

```

```

5 - (PAGTLF*SIN(ALPHINF1 - ERPVLF)*(1.0 - FEPA)
6 - ELTPALF*SIN(ALPHINF1 - ERPVLF) - ZLEFVL*CCS(ALPHINF1 - ERPVLF)
7 - (1.0 - FEPA) )*.7T
PPALF = PMACWFA + PMACTFA + PMINGLF + FVALILF
CPALF = PMCALF / ((PMJ)/2.0)*MARPV*CEAER*((VRPVF)**2.0))
XXXXXXXXXXXXXXXXXXXXXXXXXXXX
XXXXX OUTFLT FOR-ATS XXXXX
XXXXXXXXXXXXXXXXXXXXXXXXXXXX
PRINT 0333
8000 FORMAT(15X, ' * FLIGHT CONDITIONS OF THE FFW')
PRINT 0331
8001 FORMAT( ' * STEADY LEVEL FLIGHT IN FREE STREAM.')
PRINT 0332, VRFVF
8002 FORMAT( ' * FLIGHT VELOCITY (FT/SEC) IS ', F15.7)
PRINT 0533, CAPCLF
6503 FORMAT( ' GAMMA C FOR THE FFW (FREE STREAM VALUE) IS', F2(,7),
1 ' * SQUARE FEET PER SECOND.')
PRINT 0333, ALPHINFU
8003 FORMAT( ' * ANGLE OF ATTACK (DEG) IS ', F15.7)
PRINT 0334, CLINF1
8004 FORMAT( ' * COEFFICIENT OF LIFT IS ', F15.7)
PRINT 0533, ZL-FVL
5503 FORMAT( ' * THE FREE STREAM LIFT OF THE FFW WING (LBS) IS ',
1 ' F15.7)
PRINT 0535, ZL-FVIL
5505 FORMAT( ' * THE FREE STREAM LIFT OF THE FFW TAIL (LBS) IS ', F15.7)
PRINT 0534, TOLLIFT
5504 FORMAT( ' * THE FREE STREAM LIFT OF THE FFW IS', F15.7,
1 ' * POUNDS.')
PRINT 0335, CCI
8005 FORMAT( ' * COEFFICIENT OF DRAG IS ', F15.7)
PRINT 0533, TOLCDRAG
6508 FORMAT( ' THE FREE STREAM DRAG ON THE FFW IN POUNDS IS ', F15.7)
PRINT 0336, TI
8006 FORMAT( ' * THUST F.S. LEVEL (LBS) ', F15.7)
PRINT 0513, FCMFOL
6513 FORMAT( ' THE FREE STREAM POWER REQUIRED FOR FFW (FT-LB/SEC) IS',
1 ' F2(,7)
PRINT 0511, MFL
6511 FORMAT( ' THE HORSEPOWER REQUIRED IS ', F15.7)

```

69

70

(1.0 - (P1 / G1))

COMPUTING THE COMPONENT OF INDUCED VELOCITY.

$$N(II) = -A1 + (P1/S) * ANS - (A1/C1) * (P2 - SK) + (1.0 - (P1/F1)) + (A1/F1) * (P2 + SR) * (1.0 - (F1/C1))$$
$$= (P1 / F1) + (A1 / F1) * (P2 * SR) * (1 - (F1 / (1)))$$

```
0000000000 FORTIFICATION VELOCITY LEVEL FLIGHT. 0000000000
V=EL(II) = SQRT( (AOS(U(II))**2.C) + (ARS(V(II))**2.C) )
+ (ARS(W(II))**2.C)
```

THE "FREE STREAM" VELOCITY OF THE AFW IS THE VECTOR SUM OF THE AFW'S FREE STREAM VELOCITY AND THE MOTIFSHIP INDUCED VELOCITY.

$$VREFL(II) = SQRT(ATS(VMPVF + U(II)) * 2.0 + AQS(V(II)) * 2.0 + AQS(W(II)) * 2.0)$$

(0200(111)M)507 •

END OF INLCDF VELOCITY FIELD COMPLETIONS

EFFECT OF INDUCTED VELOCITY FIELD CALCULATIONS

COMPUTING THE VARIATION OF AERODYNAMIC FORCES ON THE REV
APPROACHING THE TOTALSHIP.

COMPUTING THE AERODYNAMIC FORCES ON THE RPV AT THE CENTER OF THE RPV WING AS REPRESENTATIVE. THE MID POINT OF THE RPV WING IS AT $FZ = 0.09$. THIS CORRESPONDS TO $II = 3$.

Calculating The Lift And Induced Drag Variation As The Ffv Affected

```

C
C THE MOTHERSHIP.
EP(II) = ATAN ( W(II) / ARS(UINF) )
LPC(II) = LP(II) / 0.0174533

C
C THE STRENGTH OF THE CIRCULATION (GAPCR) AROUND THE CENTER OF THE RVF
WING (ROUND VCTEX) IS BASED ON THE RELATIVE VELOCITY AT THE RVF WING.
CAPCR(II) = (2.0*WRFV) / (PI*SRPV*RC*VREL1(II))

C
C THE COMBINED VELOCITY FROM THE RVF (CLASHF) IS CALCULATED FOR
AN ELLIPTIC WING FROM EQUATION 13.23 P. 343 IN HOUGHTON.
CAPCR(II) = CAPCR(II) / (4.0*SRPV)
EPF(II) = ATAN ( CLASHF(II) / VREL1(II) )
WRFV(II) = WRFV(II) / 0.0174533

C
C ***** RVF IN LEVEL FLIGHT *****
C ***** STREAM VELOCITY VECTOR *****
C
C COMPLETING WING CL, LIFT, CD, DPAG.
CL(II) = ARFV*ALP1(II)
ZLRFV(II) = (RMC/2.0)*WRFV*ARFV*ALP1(II)*(AUS(VREL1(II))*2.0)
CC(II) = CCC + CK*(ARS(CLT3(II))*2.0)
CRCT(II) = (RMC/2.0)*WRFV*(ARS(VREL1(II))*2.0)*CC3(II)
CLT3(II) = ARFV * (ALP1(II) + TINCIC - ERFV(II))
ZLRFV(II) = (RMC/2.0) * TAPRV * (ARS(VREL1(II))*2.0)*(CLT3(II)
CC3(II) = CUCT + CKT * (ARS(CLT3(II))*2.0)
CRCT(II) = (RMC/2.0)*TAPRV*(ARS(VREL1(II))*2.0)*CC3(II)
1 + WRFV * SIN( TAL(II) )
ZLIFT(II) = ZLRFV(II) + ZLRFV(II)*COS(ERFV(II))
1 - CACT3(II)*SIN(ERFV(II))
CRAC(II) = CRAC3(II) - (ZLRFV(II)*SIN(ERFV(II)))
1 + (CRAC3(II)*COS(ERFV(II)))
C POTENTIAL INFLUENCE IMPACT.

```

```

V2(II) = DRAG(II)
C PCIPERSHIP INFLUENCE POWER.
PCAREQ3(II) = V2(II)*VREL1(II)
C PCIPERSHIP INFLUENCE MCKSPCWER.
PES(II) = PCAREQ3(II) / 550.0
C COMPUTING THE STATIC PITCH MOMENT.
FITCMLP(II) = FITPALW + FITACT
1 * (ZLRPV3(II)*CCS(ALP1(II)) + DRAG3(II)*SIN(ALP1(II)))
2 * (M - HMR3)*CEARR
3 * (ZLRPV1(II)*SIN(ALP1(II)) - DRAG1(II)*COS(ALP1(II)))**2
4 * (ZLRPV2(II)*CCS(ALP1(II)) - LREV(II)) + DRAG2(II)*SIN(ALP1(II))
5 * (LREV(II))*PACT - (M-HMR3)*CEARR
6 * (DRAG1(II)*CCS(ALP1(II)) - LREV(II))
7 * (ZLRPV3(II)*SIN(ALP1(II)) - LREV(II))*ZT
C COMPUTING PITCHING MOMENT COEFFICIENT.
CPAL(II) = PITCH-L(II) / ((RHO/2.0)*(AES(VREF)*2.0)*WREFV*CEARR)
C COMPUTING THE PARTIAL DERIVATIVES.
FLPAL(II) = (RHO/2.0)*WREFV*ARV*ZLRVREL1(II)**2.0
FLPAL(II) = RHO*CK*ARPV**2.0*ALF1(II)*(ARS(VREL1(II))*2.0)
FLPAL(II) = (RHO/2.0)*LREV*ARPV*(1.0 - FLPA)
1 * (ABS(VREL1(II)))**2.0
FLPAL(II) = RHO*CK*ARPV*CKT*(ARPV**2.0)*(ALF1(II) + YINCL0
1 - LREV(II)) * (1.0 - FLPA)
C COMPUTING DERIVATIVE OF PITCH MOMENT WITH RESPECT TO ANGLE OF ATTACK.
FPAI(II) =
1 * (FLPAL(II)*CCS(ALP1(II)) - ZLRPV3(II)*SIN(ALP1(II))
2 * (ZLRPV1(II)*SIN(ALP1(II)) + DRAG3(II)*CCS(ALP1(II)))
3 * (M - HMR3)*CEARR
4 * (FLPAL(II)*SIN(ALP1(II)) + ZLRPV3(II)*CCS(ALP1(II))
5 * (FLPAL(II)*COS(ALP1(II)) + DRAG1(II)*SIN(ALP1(II)))**2
6 * (FLPAL(II)) =
1 * (FLPAL(II)*CCS(ALP1(II)) - LREV(II)) - ZLRPV3(II)*
2 * (SIN(ALP1(II)) - LREV(II))*(1.0 - FLPA) + FOPAL(II)*SIN(
3 * ALF1(II) - LREV(II)) + DRAG3(II)*CCS(ALP1(II)) - LREV(II))*(1.0
4 * (FLPA))*(FLPA - (M - HMR3)*CEARR)
5 * (FLPAL(II)*CCS(ALP1(II)) - LREV(II)) - DRAG1(II)*SIN(ALP1(II))
6 * (LREV(II))*(1.0 - FLPA) - PLPAL(II)*SIN(ALP1(II)) - LREV(II))
7 * (ZLRPV3(II)*CCS(ALP1(II)) - LREV(II))*(1.0 - FLPA))**2
FPAI(II) = FPAI(II) + PMCPA + FPAI(II) + FPAI(II)
CPAL(II) = FPAI(II) / ((RHO/2.0)*WREFV*CEARR*(ABS(VREFV)**2.0))

```


**Reproduced from
best available copy.**

[illegible]

[illegible]

[illegible]

```

      ((((( DRAW 0.5 X 11 BOX (((((
      CALL PLOT ( -3.02, -1.77, 3)
      CALL PLOT ( 0.02, -1.77, 2 )
      CALL PLOT ( 0.02, 6.77, 2 )
      CALL PLOT ( -3.02, 6.77, 2 )
      CALL PLOT ( -3.02, -1.77, 2 )
      CALL PLOT ( 12.02, -5.1, -3)
      ((((( PLOT CF CHA VERSES P (((((

```

```

      ((((( PLOT CF CHA VERSES P (((((

```

```

      CALL PLOT ( 1.0, 1.75, -3)
      CALL SCALE ( CHA , SCALY, KP, KS )
      CALL AXIS ( 6.0, 0.0, 10, -1, SCALEX, 00.0, F(KP+1), P(KF+2) )
      CALL AXIS ( 0.0, 0.0,
      1 27M SLOPE OF CM VS ALPHA CURVE, 27,
      2 SCALY, 5.00, CHA(KP+1), CHA(KF+2) )
      CALL SYMOL ( 0.10, -0.570, 0.143,
      1 36M PPV LOCATION / 101 FRESH WING SPAN, 0.0, 36 )
      CALL LINE ( P , CHA , KP, 1, 1, 11 )
      CALL SYMOL ( 1.50, 5.00, 0.105,
      1 40PPV SPAN / FCFRESH SPAN = 0.1502 , 30.0, 40 )
      CALL SYMOL ( 1.51, 4.75, 0.105,
      1 40PHOT-FRESH VELOCITY = 300.0 KNOTS, 00.0, 40 )
      CALL SYMOL ( 1.51, -0.50, 0.105,
      1 40INITIAL CLOSING VELOCITY = 5.0 KNOTS, 30.0, 40 )
      ((((( DRAW BOX (((((
      CALL PLOT ( -3.75, -0.75, 3 )
      CALL PLOT ( 7.00, -0.75, 2 )
      CALL PLOT ( 7.00, 5.60, 2 )
      CALL PLOT ( -0.75, 5.60, 2 )
      CALL PLOT ( -0.75, -0.75, 2 )

```

```

      ((((( DRAW 0.5 X 11 BOX (((((
      CALL PLOT ( -3.02, -1.77, 3)
      CALL PLOT ( 0.02, -1.77, 2 )
      CALL PLOT ( 0.02, 6.77, 2 )
      CALL PLOT ( -3.02, 6.77, 2 )
      CALL PLOT ( -3.02, -1.77, 2 )
      CALL PLOT ( 12.02, -5.1, -3)

```

```

C
C
      ((((( PLOT OF T VERSES P (((((
      CALL PLOT ( 1.00, 1.75, -3)
      CALL SCALE ( T , SCALEY, KP, MS )
      CALL AXIS (0.00,0.00,1H , -1,SCALEX, 00.00,P(KP+1),P(KP+2))
      CALL AXIS(0.00,0.00,
      1 22H KPV THRUST / FREE STREAM THRUST, 22,
      2 SCALEY,00.00,
      3 466:: 11A (21V2))
      CALL SYMBOL(00.100,-0.070,0.140,
      1 22H KPV LOCATION / WOTERSHIP WING SPAN, 00.0, 36 )
      CALL LINE( P , T , KP, 1, 1, 11)
      CALL SYMBOL ( 2.00, 5.00, 0.105,
      1 40H WING SPAN / WOTERSHIP SPAN = 6.15002 , 00.0, 40)
      CALL SYMBOL ( 2.00, -0.75, 0.105,
      1 40H WOTERSHIP VELOCITY = 300.0 KNOTS, 00.0, 40 )
      CALL SYMBOL ( 2.00, -0.50, 0.105,
      1 40H INITIAL CLOSING VELOCITY = 5.0 KNOTS, 00.0, 40 )
      ((((( DRAW BOX (((((
      CALL PLOT ( -0.75, -0.75, 3 )
      CALL PLOT ( 7.00, -0.75, 2 )
      CALL PLOT ( 7.00, 5.60, 2 )
      CALL PLOT ( -0.75, 5.60, 2 )
      CALL PLOT ( -0.75, -0.75, 2 )
      ((((( DRAW 0.5 X 11 BOX (((((
      CALL PLOT ( -1.02, -1.77, 3)
      CALL PLOT ( 6.02, -1.77, 2 )
      CALL PLOT ( 6.02, 6.77, 2 )
      CALL PLOT ( -3.02, 6.77, 2 )
      CALL PLOT ( -3.02, -1.77, 2 )
      CALL PLOT (12.10, -5.0, -3)
      ((((( PLOT OF WELP VERSES P (((((
      CALL PLOT ( 1.00, 1.75, -3)
      CALL SCALE ( WELP , SCALEY, KP, MS )
      CALL AXIS (0.00,0.00,1H , -1,SCALEX, 00.00,P(KP+1),P(KP+2))
      CALL AXIS(0.00,0.00,
      1 22H KPV VELOCITY / WOTERSHIP VELOCITY, 35,

```



```

CALL SY497L ( 1.50, 4.50, 0.105,
1 40INITIAL CLOSING VELOCITY = 5.0 KNOTS, 00.0, 40 )
      ((( ( DRAW EX ( (((
CALL PLOT ( -0.75, -0.75, 3 )
CALL PLOT ( 7.00, -0.75, 2 )
CALL PLOT ( 7.00, 5.50, 2 )
CALL PLOT ( -0.75, 5.50, 2 )
CALL PLOT ( -0.75, -0.75, 2 )

      ((( ( DRAW 2.5 X 11 70X ((( (
CALL PLOT ( -3.02, -1.77, 3 )
CALL PLOT ( 3.02, -1.77, 2 )
CALL PLOT ( 3.02, 6.77, 2 )
CALL PLOT ( -3.02, 6.77, 2 )
CALL PLOT ( -3.02, -1.77, 2 )
CALL PLOT ( 12.00, -5.00, -3 )

      ((( ( PLOT OF CL V-USES P ((( (
CALL PLOT ( 1.00, 1.75, -3 )
CALL SCALE ( CL , SCALE, KP, MS )
CALL AXIS ( 0.00, 0.00, 10, -1, SCALEX, 00.00, P(MP+1), P(VF+2) )
CALL AXIS ( 0.00, 0.00,
1 24H KP CL / FREE STREAM CL, 24,
2 SCALEY, 50.00,
3 CL(MP+1), CL(MP+2) )
CALL SY497L ( 0.100, -0.570, 0.140,
1 24H KP LOCATION / MEMBERSHIP WING SPAN, 00.0, 36 )
      CALL LINE ( P , CL , KP, 1, 1, 11 )
CALL SY497L ( 1.50, 5.00, 0.105,
1 40REF SPAN / MEMBERSHIP SPAN = 0.1500 , 00.0, 40 )
CALL SY497L ( 1.50, 4.75, 0.105,
1 40MEMBERSHIP VELOCITY = 300.0 KNOTS, 00.0, 40 )
CALL SY497L ( 1.50, 4.50, 0.105,
1 40INITIAL CLOSING VELOCITY = 5.0 KNOTS, 00.0, 40 )
      ((( ( DRAW EX ((( (
CALL PLOT ( -0.75, -0.75, 3 )
CALL PLOT ( 7.00, -0.75, 2 )
CALL PLOT ( 7.00, 5.50, 2 )
CALL PLOT ( -0.75, 5.50, 2 )

```

```

C
C
CALL PLOT ( -0.75, -0.75, 2 )
  ((((( DRAW 0.5 X 11 BOX (((((
  CALL PLOT ( -3.02, -1.77, 3 )
  CALL PLOT ( 0.02, -1.77, 2 )
  CALL PLOT ( 0.02, 6.77, 2 )
  CALL PLOT ( -3.02, 6.77, 2 )
  CALL PLOT ( -3.02, -1.77, 2 )
  CALL PLOT ( 12.00, -5.00, -3 )

C
C
  ((((( PLOT CF ALP VERSES P (((((
  CALL SCALE ( ALP , SCALEY, KP, KS )
  CALL PLOT ( 1.00, 1.75, -3 )
  CALL AXIS ( 0.00, 0.00, 14, -1, SCALEX, 00.00, (F(RP+1), P(KF+2))
  CALL AXIS ( 0.00, 0.00,
  1 2EM ALPHA / FREE STREAM ALPHA, 26,
  2 SCALEY, 50.00,
  3 ALP(KP+1), ALP(KF+2))
  CALL SYMOL ( 0.00, 0.00, -0.07, 0.00, 140,
  1 2EM RPV LOCATION / 40THRESHIP WING SPAN, 00.00, 36 )
  CALL LINE ( P , ALP , KP, 1, 1, 11 )
  CALL SYMOL ( 1.00, 0.00, 0.105,
  1 40THRESHIP SPAN / 40THRESHIP SPAN = 0.15002 , 00.00, 40 )
  CALL SYMOL ( 1.50, 4.75, 0.105,
  1 40THRESHIP VELOCITY = 300.0 KNOTS, 00.00, 40 )
  CALL SYMOL ( 1.00, 0.50, 0.105,
  1 40THRESHIP CLOSING VELOCITY = 5.0 KNOTS, 00.00, 40 )
  ((((( DRAW BOX (((((
  CALL PLOT ( -0.75, -0.75, 3 )
  CALL PLOT ( 7.00, -0.75, 2 )
  CALL PLOT ( 7.00, 5.00, 2 )
  CALL PLOT ( -0.75, 5.00, 2 )
  CALL PLOT ( -0.75, -0.75, 2 )

C
C
  ((((( DRAW 0.5 X 11 BOX (((((
  CALL PLOT ( -3.02, -1.77, 3 )
  CALL PLOT ( 0.02, -1.77, 2 )
  CALL PLOT ( 0.02, 6.77, 2 )
  CALL PLOT ( -3.02, 6.77, 2 )

```

```

CALL PLOT (-3.02, -1.77, 2)
CALL PLOT (12.00, -5.3, -3)

      ((((( PLOT CF TAU VERSES P (((((
CALL PLOT ( 1.00, 1.75, -3)
CALL SCALE ( TAL , SCALEY, KP, MS )
CALL AXIS (0.00,0.00,10 ,1,SCALEX, 00.00,P(MF+1),P(KP+2))
CALL AXIS(0.00,0.00,
1 304 INDUCED ANGLE OF ATTACK (DEG), 30,
      SCALEY,00.00,
2
3 TAL(PD+1), TAL(KP+2))
CALL SYMBOL(00.100,-0.57(0.140,
1 304 PIV LOCATION / WINGSPAN WING SPAN, 00.0, 36 )
CALL LINE( F , TAU , KP, 1, 11)
CALL SYMBOL ( 1.50, 5.00, 3.105,
1 400 PIV SPAN / WINGSPAN SPAN = (.15000 + 00.0, 40)
CALL SYMBOL ( 1.50, 4.75, 3.105,
1 400 WINGSPAN VELOCITY = 300.0 MACIS, 00.0, 40 )
CALL SYMBOL ( 1.50, 4.50, 3.105,
1 400 INITIAL CLOSING VELOCITY = 5.0 MACIS, 00.0, 40 )
      ((((( OPAN FCX (((((
CALL PLOT ( -0.75, -3.75, 3 )
CALL PLOT ( 7.00, -0.75, 2 )
CALL PLOT ( 7.00, 5.50, 2 )
CALL PLOT ( -0.75, 5.50, 2 )
CALL PLOT ( -0.75, -3.75, 2 )

      ((((( OPAN 2.5 X 11 BOX (((((
CALL PLOT ( -3.02, -1.77, 3)
CALL PLOT ( 8.00, -1.77, 2 )
CALL PLOT ( 8.00, 6.77, 2 )
CALL PLOT ( -3.02, 6.77, 2 )
CALL PLOT ( -3.02, -1.77, 2 )
CALL PLOT (12.00, -5.3, -3)

      ((((( PLOT CF CD VERSES P (((((
CALL PLOT ( 1.00, 1.75, -3)
CALL SCALE ( CD , SCALEY, KP, MS )

```

UUU

```

CALL LINE( P , CLOSEVP, KP, 1, 1, 11)
CALL SYMOL ( 2.00, 2.00, 0.105,
1 400REV SPAN / MOTHERSHIP SPAN = 0.15002 , 00.0, 40 )
CALL SYMOL ( 2.00, 1.75, 0.105,
1 400MOTHERSHIP VELOCITY = 300.0 KNOTS, 00.0, 40 )
CALL SYMOL ( 2.00, 1.50, 0.105,
1 400INITIAL CLOSING VELOCITY = 5.0 KNOTS, 00.0, 40 )
((((( ORAN EX (((((
CALL PLOT ( -0.75, -0.75, 1 )
CALL PLOT ( 7.00, -0.75, 2 )
CALL PLOT ( 7.00, 5.60, 2 )
CALL PLOT ( -0.75, 5.60, 2 )
CALL PLOT ( -0.75, -0.75, 2 )
((((( ORAN 4.5 X 11 BOX ((((((
CALL PLOT ( -3.02, -1.77, 3)
CALL PLOT ( 8.02, -1.77, 2 )
CALL PLOT ( 8.02, 6.77, 2 )
CALL PLOT ( -3.02, 6.77, 2 )
CALL PLOT ( -3.02, -1.77, 2 )
CALL PLOT ( 12.00, -5.0, -3)
((((( PLOT OF TIMEP VERSES P ((((((
CALL PLOT ( 1.00, 1.75, -3)
CALL SCALE ( TIMEP , SCALEV, KP, MS )
CALL AXIS ( 0.0, 11.00, 1M , -1, SCALEX, 0.00, P(KP+1), P(KP+2))
CALL AXIS ( 0.00, 0.00,
1 1ST TIME TO EOCK (SEC), 10, SCALEV, 50.00,
2 TIMEP(KP+1), TIMEP(KP+2))
CALL SYMOL( 1.00, -0.570, 0.140,
1 200 REV LOCATION / MOTHERSHIP KING SPAN, 0(0, 36 )
CALL LINE( P , TIMEP , KP, 1, 1, 11)
CALL SYMOL ( 1.50, 5.00, 0.105,
1 400REV SPAN / MOTHERSHIP SPAN = 0.15002 , 00.0, 40 )
CALL SYMOL ( 1.50, 4.75, 0.105,
1 400MOTHERSHIP VELOCITY = 300.0 KNOTS, 00.0, 40 )
CALL SYMOL ( 1.50, 4.50, 0.105,
1 400INITIAL CLOSING VELOCITY = 5.0 KNOTS, 00.0, 40 )

```

```

C      (CCCC DRAN RCX (CCCC
CALL FLOT (-0.75, -0.75, 3)
CALL FLOT (7.00, -0.75, 2)
CALL FLOT (7.00, 5.50, 2)
CALL FLOT (-0.75, 5.50, 2)
CALL FLOT (-0.75, -0.75, 2)

C      (CCCC DRAN P.5 X 11 BOX (CCCC
CALL FLOT (-3.00, -1.77, 3)
CALL FLOT (8.00, -1.77, 2)
CALL FLOT (3.00, 6.77, 2)
CALL FLOT (-3.00, 6.77, 2)
CALL FLOT (-3.00, -1.77, 2)
CALL FLOT (8.00, -1.77, 2)

C      CC TO 9110
9000 CONTINUE
C      *****
C      ***** END OF PLOTTING *****
C      *****
C      STOP
C      END

```

```

SUBROUTINE FNEVAL (X,FX)
  COMMON P1, P2, P3, S
C      ***** PART OF INTEGRATION ROUTINE, COMPUTES THE VALUE OF THE FUNCTION IN
C      THE INTEGRAL.
C      ***** P1 = SQR ((ABS(S) ** 2.0) - (ABS (Y) ** 2.0))
C      ***** P1 = (( (ABS(P1) ** 2.0) + (ABS (P2 - Y) ** 2.0)
C      ***** 1 + (P1**2) ** 2.0) ** 1.5)
      Y = X
      P1 = SQR ((ABS(S) ** 2.0) - (ABS (Y) ** 2.0))
      P1 = (( (ABS(P1) ** 2.0) + (ABS (P2 - Y) ** 2.0)
      1 + (P1**2) ** 2.0) ** 1.5)
      P2 = 11 / C1
      RETURN

```

EAC

```

SUBROUTINE SIMPS(A,R,TOL,J,JMIN,ANSM,ALARM,JTCL)
C SIMPS IS A LIBRARY SUBROUTINE.
C SIMPS INTEGRATION SUBROUTINE
C CALLING SEQUENCE
C CALL SIMPS(A,R,TOL,JMIN,ANSM,ALARM,JTCLN)
C A=LOWER LIMIT
C B=UPPER LIMIT
C TOL=10**S MEANS S SIGNIF. DIGITS
C NMAX=NO. OF ITERATIONS ALLOWED
C JMIN=MIN NO. OF ITERATIONS
C ANSM=VALUE OF INTEGRAL
C ALARM=.J. INDICATES CONVERGENCE
C          =1. OTHERWISE
C          JTCL=NO. OF ITERATIONS REQUIRED FOR CONVERGENCE
C SIMPS REQUIRES SETTING OF SUBROUTINE FNEVAL TO EVALUATE INTEGRAL
C FORPAT(///10X,24H-INTEGRAL DID NOT CONVERGE AFTER,
1 12X,15,2X,10H-ITERATIONS///)
C IF (A-B) 15,16,15
10 C=C*0
C 10 75
15 ALARM=0.0
JTCL=1
IF (F-A)
CALL FNEVAL(A,F)
CALL FNEVAL(B,F)
FNEVAL EVALUATES INTEGRAND AT SPECIFIED POINTS
F=F*F3
F=F*F
20 IF=F*F
S=C*0
C=F*2.0
AC=F*0.
X=AC
30 CALL FNEVAL(X,F)
S=S+F*F

```

SIMPS001
SIMPS002
SIMPS003
SIMPS004
SIMPS005
SIMPS006
SIMPS007
SIMPS008
SIMPS009
SIMPS010
SIMPS011
SIMPS012
SIMPS013
SIMPS014
SIMPS015
SIMPS016
SIMPS017
SIMPS018
SIMPS019
SIMPS020
SIMPS021
SIMPS022
SIMPS023
SIMPS024
SIMPS025
SIMPS026
SIMPS027
SIMPS028
SIMPS029
SIMPS030
SIMPS031
SIMPS032
SIMPS033
SIMPS034

Reproduced from
best available copy.

SIMFS025
SIMFS026
SIMFS027
SIMFS028
SIMFS029
SIMFS030
SIMFS031
SIMFS032
SIMFS033
SIMFS034
SIMFS035
SIMFS036
SIMFS037
SIMFS038
SIMFS039
SIMFS040
SIMFS041
SIMFS042
SIMFS043
SIMFS044
SIMFS045
SIMFS046
SIMFS047
SIMFS048
SIMFS049
SIMFS050
SIMFS051
SIMFS052

```

PC=END*RM
IF (AN-D) JJ,40,40
ER=FL+4.J*S
EL=FL+2.J*S
PA=C
EPX2=2.J*RM
EP2)=A+X1(6K,PPX2)
IF (AES(13-JPX2)-AES (OMAX)*TOL) 70,70,50
J1CL=J1OL+1
IF (J1CL-J1OL,65,65
CC TO 27
60 ES PRINT 1,J
ALAPM=1.0
FETLEN
70 IF (J1CL-J1IN) 50,75,75
75 ASB=6K*7/3.0
FETLEN
ENC

```

Vita

Jon L. Gross was born [REDACTED]

He graduated from [REDACTED] [REDACTED] Missouri, in 1962. He graduated from the University of Illinois in 1967 with a Bachelor of Science degree in Aeronautical and Astronautical Engineering. He obtained a commission in the United States Air Force through R.O.T.C., and went on active duty immediately following graduation.

This thesis was typed by Miss Sherry L. Willman.